

1 **A first-in-class inhibitor of apicomplexan FtsH1 disrupts plastid biogenesis in**
2 **human pathogens**

3
4 Katherine Amberg-Johnson^{1,3}, Sanjay B. Hari⁴, Suresh M. Ganesan⁵, Hernan A. Lorenzi⁶,
5 Robert T. Sauer⁴, Jacquin C. Niles⁵, Ellen Yeh^{1,2,3,*}

6
7 ¹Department of Biochemistry, ²Pathology, and ³Microbiology and Immunology, Stanford
8 Medical School

9 ⁴Department of Biology, Massachusetts Institute of Technology

10 ⁵Department of Biological Engineering, Massachusetts Institute of Technology

11 ⁶Department of Infectious Disease, The J. Craig Venter Institute

12 *Corresponding author

13
14 **The malaria parasite *Plasmodium falciparum* and related apicomplexan pathogens**
15 **contain an essential plastid organelle, the apicoplast, which is a key anti-parasitic**
16 **target. Apicoplast biogenesis depends on novel, but largely cryptic, mechanisms for**
17 **protein/lipid import and organelle inheritance during parasite replication. These**
18 **critical pathways present untapped opportunities to discover new parasite-specific**
19 **drug targets. We used an innovative screen to identify the natural product actinonin**
20 **as a first-in-class antimalarial compound inhibiting apicoplast biogenesis. Resistant**
21 **mutation, chemical-genetic interaction, and biochemical inhibition demonstrate that**
22 **the unexpected target of actinonin in *P. falciparum* and *Toxoplasma gondii* is FtsH1,**
23 **a homolog of a bacterial membrane AAA+ metalloprotease. *PfFtsH1* is the first**
24 **novel factor required for apicoplast biogenesis identified in an unbiased screen. Our**
25 **findings demonstrate that FtsH1 is a novel and, importantly, druggable antimalarial**
26 **target. Development of FtsH1 inhibitors will have significant advantages over**
27 **existing apicoplast-targeting compounds with improved drug kinetics and**
28 **multistage efficacy against multiple human parasites.**

29
30 **Introduction**

31 There is an urgent need for antimalarials with novel mechanisms-of-action to
32 combat resistance to frontline drugs. The apicoplast is a plastid organelle uniquely found
33 in *Plasmodium* parasites that cause malaria and related apicomplexan pathogens^{1,2}.
34 Though non-photosynthetic, the apicoplast is required for the biosynthesis of essential
35 metabolites in the organisms that retained it³⁻⁹. Acquired by a secondary eukaryote-
36 eukaryote endosymbiosis, it utilizes bacterial and organellar pathways distinct from those
37 of mammalian host cells. Given its unique and essential biology, the apicoplast is an ideal
38 source of parasite-specific drug targets that minimize host off-target toxicity.

39 Despite its biomedical potential, broadly effective antimalarials targeting the
40 apicoplast have been elusive. The first class of apicoplast inhibitors to be identified was
41 drugs like doxycycline, clindamycin, and chloramphenicol that block prokaryotic protein
42 synthesis^{10,11}. The antimalarial effects of these clinically-approved antibiotics were
43 noticed well before they were shown to inhibit the bacterial-like ribosome in the
44 apicoplast¹². Unfortunately translation inhibitors cause a characteristic “delayed death” *in*
45 *vitro* in which parasite growth inhibition occurs in the second replication cycle after drug
46 treatment. The delayed effect is related to their mechanism-of-action and is also seen with

47 DNA replication and transcription inhibitors that block apicoplast gene expression.
48 Delayed death manifests as a slow onset-of-action of translation inhibitors that limits
49 their antimalarial efficacy and clinical use.

50 The next druggable targets in the apicoplast were several prokaryotic metabolic
51 pathways. Fosmidomycin, an inhibitor of MEP isoprenoid precursor biosynthesis in the
52 apicoplast, causes parasite growth inhibition in a single replication cycle *in vitro* and
53 rapid parasite clearance in human clinical trials^{3,13-15}. Unfortunately initial parasite
54 clearance is followed by recrudescence infections in 50% of patients. These treatment
55 failures have brought into question the clinical utility of fosmidomycin and other MEP
56 inhibitors. Yet despite the expectation that the apicoplast would serve many essential
57 functions, we showed that only isoprenoid precursor biosynthesis is required during the
58 symptomatic blood stage of *Plasmodium*⁸. The apicoplast's limited function in blood-
59 stage *Plasmodium* precludes opportunities to target alternative metabolic pathways.

60 Clearly the pipeline for essential and druggable apicoplast targets has run dry.
61 New approaches are needed to identify drug targets that avoid the known liabilities of
62 targeting apicoplast gene expression and metabolism. Until now, identification of drug
63 targets in the apicoplast has been based on conserved bacterial and primary chloroplast
64 pathways whose functions can be inferred from model organisms. However, many
65 essential pathways for protein/lipid import into the apicoplast and organelle inheritance
66 during parasite replication will be unique to secondary plastids and evolutionarily
67 divergent from model eukaryotic biology^{16,17}. Drug targets in these organelle biogenesis
68 pathways are likely to be 1) essential to parasite survival, even in the context of the
69 apicoplast's drastically reduced metabolic function, 2) required for all proliferative stages
70 of the parasite life cycle, and 3) conserved across apicomplexan parasites. Thus
71 apicoplast biogenesis represents a promising but unexplored frontier in antimalarial drug
72 discovery.

73 While forward genetic screens have been extremely powerful in uncovering novel
74 cellular pathways in model organisms, they are not currently tractable in *Plasmodium*. To
75 circumvent these limitations, we took a chemical-genetic approach from phenotypic
76 screening to target identification. We first identified the natural product actinonin as a
77 novel inhibitor of apicoplast biogenesis. We then uncovered the essential role of the
78 membrane metalloprotease FtsH1 in organelle biogenesis in apicomplexan pathogens.
79 FtsH1 is a druggable target in apicoplast biogenesis that offers advantages over the
80 mechanisms-of-action of existing apicoplast inhibitors and has a ready hit compound to
81 pursue drug development.

82

83 **Results**

84

85 **Identification of a novel apicoplast biogenesis inhibitor**

86 We screened >400 growth-inhibitory antimalarial compounds with unknown
87 mechanisms-of-action to identify novel inhibitors of apicoplast biogenesis (Extended
88 Data Table 1)¹⁸⁻²². Our selection criteria aimed to identify compounds that 1) caused
89 parasite growth inhibition (essential target) in a single replication cycle (avoiding delayed
90 death), 2) were specific in their disruption of the apicoplast, and 3) resulted in loss of the
91 apicoplast during parasite replication. This unique inhibition phenotype distinguished

92 selected compounds from known apicoplast gene expression or metabolism inhibitors,
93 ensuring discovery of a novel class of inhibitors.

94 A single natural product antibiotic, actinonin, matched our criteria²³. Consistent
95 with its reported antimalarial activity, actinonin caused *P. falciparum* growth inhibition
96 in a single replication cycle ($EC_{50} = 3.2 \mu\text{M}$; 95% CI 2.5-4.1)^{19,24}. Because isoprenoid
97 precursor biosynthesis is the only essential function of the apicoplast in blood-stage *P.*
98 *falciparum*, any disruption of the apicoplast, including complete loss of the organelle, can
99 be rescued by addition of the isoprenoid precursor, isopentenyl pyrophosphate (IPP), in
100 the growth media⁸. Indeed actinonin's EC_{50} shifted nearly 20-fold in the presence of IPP
101 to $61 \mu\text{M}$ (95% CI 50-75). Although the translation inhibitor chloramphenicol also
102 caused growth inhibition rescued by IPP, parasite growth inhibition and resulting
103 apicoplast biogenesis defects were delayed by one replication cycle following drug
104 treatment (Extended Data Fig. 1b and 2a,c). Compared to chloramphenicol, actinonin
105 clearly had more rapid antimalarial activity. These results demonstrate that actinonin
106 specifically inhibits the apicoplast without a delayed death phenotype (Fig. 1a; Extended
107 Data Fig. 1a; Extended Data Table 1).

108 Previously actinonin was observed to cause a block in the morphologic
109 development of the apicoplast during parasite replication²⁴. However, these defects were
110 observed without IPP growth rescue when parasite replication was also inhibited. Absent
111 IPP rescue, the MEP inhibitor fosmidomycin also showed a block in apicoplast
112 development. Based on the observed similarities in their inhibition phenotype, the authors
113 concluded that actinonin, like fosmidomycin, inhibited apicoplast metabolism. We sought
114 to clarify these earlier observations using IPP rescue to distinguish between specific
115 apicoplast defects caused by the inhibitor and nonspecific defects observed in a non-
116 replicating parasite. Using quantitative PCR (qPCR) to detect the apicoplast genome and
117 microscopy to localize an apicoplast-targeted GFP, we show that actinonin-treated *P.*
118 *falciparum*, rescued for growth by IPP, no longer replicated their apicoplast genome and
119 produced daughter parasites lacking apicoplasts, consistent with a defect in apicoplast
120 biogenesis (Fig. 1b-c, Extended Data Fig. 2a,e)⁸. In contrast, both the copy number of the
121 apicoplast genome and apicoplast development were unaffected by fosmidomycin
122 treatment under IPP rescue, indicating that the previously reported apicoplast biogenesis
123 defects were nonspecific (Extended Data Fig 1b and 2a,d). Taken together, actinonin's
124 inhibition phenotype distinguishes it from known inhibitors that disrupt apicoplast gene
125 expression and metabolism and indicates that it has a novel mechanism-of-action in
126 organelle biogenesis (Extended Data Fig 1b and 2).

127 **Actinonin is unlikely to inhibit the peptide deformylase in *Plasmodium* parasites**

128 To identify actinonin's molecular target, we first took a candidate-based
129 approach. In bacteria and mammalian mitochondria, actinonin potently inhibits a peptide
130 deformylase (PDF) which catalyzes the co-translational removal of the formyl group
131 from nascent chains²⁵. The apicoplast translation machinery is prokaryotic in origin and
132 therefore contains a PDF. Previously actinonin was shown to inhibit the enzymatic
133 activity of purified *P. falciparum* PDF with a reported $IC_{50} = 2.5 \mu\text{M}$ ²⁶. The potency of
134 this inhibition is 10^{2-3} fold less than those reported for *E. coli* or human PDF^{25,27,28}. Given
135 the role of Pdf in apicoplast translation, its inhibition is expected to give a delayed
136 death phenotype as observed with other translation inhibitors, whereas we clearly
137

138 observed growth inhibition in a single replication cycle (Figure 1). Puzzled by this
139 inconsistency, we used both genetic and chemical approaches to ascertain whether the
140 *PfPDF* is the target of actinonin.

141 In bacteria, resistance to actinonin is conferred by overexpression of PDF²⁹. We
142 constructed a *P. falciparum* strain containing a second copy of *PfPDF*-myc in which
143 expression was regulated by tetR-DOZI-binding aptamer sequences³⁰. As expected,
144 *PfPDF*-myc expression was observed in the presence of anhydrotetracycline, which
145 disrupts the tetR-DOZI repressor-aptamer interaction (Extended Data Fig. 3A). We
146 assessed the import of overexpressed *PfPDF*-myc into the apicoplast by determining its
147 apicoplast-dependent protein cleavage. Luminal apicoplast proteins, including *PfPDF*,
148 contain an *N*-terminal transit peptide sequence that is required for trafficking to the
149 apicoplast and is cleaved upon import¹⁶. In normal parasites, *PfPDF*-myc was detected as
150 a majority processed and minority unprocessed protein (Extended Data Fig 3A-B). In
151 IPP-rescued parasites lacking their apicoplast, *PfPDF*-myc accumulates as only the
152 unprocessed protein (Extended Data Fig 3B)⁸. These results indicate that *PfPDF*-myc is
153 properly trafficked. Contrary to what is seen in bacteria, *PfPDF*-myc overexpression did
154 not confer actinonin resistance indicating that *PfPDF* may not be the target of actinonin
155 (Extended Data Fig. 3C). Because the lack of actinonin resistance may also have been
156 due to insufficient overexpression or nonfunctional *PfPDF*-myc, we attempted to
157 generate a strain with *pdf* expression regulated at the endogenous loci but were unable
158 obtain viable parasites in two separate transfections performed in parallel with successful
159 positive controls.

160 We also assessed whether the actinonin target functions downstream of the
161 ribosome, as is expected for *PfPDF*. In mitochondria, translation inhibitors suppress the
162 effects of actinonin since a block in translation supercedes a block in PDF activity³¹.
163 Similarly, we expected that if PDF was the target of actinonin leading to growth
164 inhibition in a single replication cycle, then co-treatment with chloramphenicol would
165 result in a delayed death phenotype, whereby translation inhibition would mask the
166 effects of PDF inhibition. Surprisingly, chloramphenicol did not suppress the effects of
167 actinonin (Extended Data Fig. 3D). Taken together, our results indicate that 1) actinonin
168 does not cause delayed death as would be expected for *PfPDF* inhibition, 2)
169 overexpression of *PfPDF* did not confer actinonin resistance, and 3) the effect of
170 actinonin was not suppressed by inhibition of the ribosome upstream of *PfPDF*. These
171 results are inconsistent with *PfPDF* being the target of actinonin.

172 173 **Actinonin-resistant *T. gondii* contain a mutation in *TgFtsH1***

174 Because the target of actinonin in *P. falciparum* did not appear to be conserved in
175 model organisms, we turned to an unbiased approach. Our collaborators and we
176 independently attempted to isolate actinonin-resistant *P. falciparum* but failed using
177 multiple selection methods, including chemical mutagenesis, that successfully selected
178 resistance against other compounds (Prof. David Fidock, personal communication)^{21,22}.
179 Therefore, we turned to *Toxoplasma gondii*, a related apicomplexan parasite, which
180 contains an apicoplast of the same evolutionary origin, because it is easier to grow to
181 large numbers and to genetically modify.

182 To determine whether actinonin disrupts apicoplast biogenesis in *T. gondii*, we
183 characterized its inhibition phenotype. Curiously, *T. gondii* also shows a delayed death

184 phenotype with apicoplast translation inhibition, whereby drug treatment in the first lytic
185 cycle results in parasite growth inhibition in the second cycle¹⁰. However, the mechanism
186 underlying delayed death in *T. gondii* is distinct from that in *Plasmodium*. Delayed death
187 in *T. gondii* is associated with defects in apicoplast biogenesis and formation of parasites
188 that lack apicoplasts during the first lytic cycle³²⁻³⁴. Though these “apicoplast-minus”
189 parasites are viable in the first lytic cycle, they cannot replicate in the second lytic cycle.
190 (In contrast, *Plasmodium* parasites treated with translation inhibitors exhibit apicoplast
191 biogenesis defects in the second replication/lytic cycle, wherein loss of the apicoplast
192 immediately blocks parasite replication¹¹.) Consistent with an apicoplast biogenesis
193 defect in *T. gondii*, actinonin showed delayed death growth inhibition (EC₅₀= 14 μM;
194 95% CI 13-14) with formation of apicoplast-minus parasites during drug treatment (Fig.
195 2a and Extended Fig. 4a)³².

196 Because actinonin disrupted apicoplast biogenesis in both *T. gondii* and *P.*
197 *falciparum*, suggesting a common target, we selected actinonin-resistant *T.gondii* and
198 determined the whole-genome sequences for eight independently selected clones (Fig.
199 2b). Remarkably, five clones harbored the same mutation encoding a N805S variant in
200 the metalloprotease domain of the membrane-bound AAA+ protease *TgFtsH1*
201 (TGGT1_259260) (Fig. 2d; Extended Data Table 2). *TgFtsH1* was compelling as the
202 actinonin target for two reasons. First, *TgFtsH1* localizes to the apicoplast³⁵. Second,
203 actinonin is a peptide mimetic containing a metal-binding hydroxamic acid, a class of
204 molecules that typically binds metalloproteases^{25,36}. Replacement of the endogenous
205 *TgFtsH1* locus with the allele encoding *TgFtsH1(N805S)* caused a 3.5-fold shift in the
206 actinonin EC₅₀, similar to the resistance observed in the actinonin-resistant clones (Fig.
207 2c). Notably growth inhibition at this higher actinonin concentration did not result in
208 delayed death, suggesting that actinonin no longer bound FtsH1 and growth inhibition
209 was the result of secondary targets (Extended Data Fig. 4b). In contrast, no increase in the
210 actinonin EC₅₀ was observed when the endogenous locus was replaced with the WT allele
211 (Fig. 2c). Taken together, the known metalloprotease binding of actinonin, the predicted
212 metalloprotease activity of *TgFtsH1*, and the validated actinonin-resistant mutation in
213 *TgFtsH1* support FtsH1 as the target of actinonin in *T. gondii*, providing a strong
214 candidate for validation in *P. falciparum*.

215 216 **C-terminal cleavage of the *P. falciparum* FtsH1 homolog is dependent on the** 217 **apicoplast**

218 The *P. falciparum* genome contains three FtsH homologs. One of these, *PfFtsH1*
219 (Pf3D7_1239700) is most closely related to *TgFtsH1* by phylogenetic analysis³⁷. Unlike
220 *TgFtsH1*, *PfFtsH1* was previously reported to localize to mitochondria, not the
221 apicoplast³⁷. However the same study reported that, like *TgFtsH1*, *PfFtsH1* undergoes
222 processing. The mitochondrial localization was most clearly demonstrated for the C-
223 terminally tagged fragment, but the localization of the N-terminal fragment containing the
224 ATPase and protease domains was unclear. Proteins required for apicoplast biogenesis
225 may localize to various cellular compartments outside of the apicoplast. For example,
226 both the dynamin DrpA and Atg8 required for apicoplast biogenesis are cytoplasmic
227 proteins, whereas apicoplast protein trafficking machinery is likely to exist in the ER^{32,34}.
228 Close association of the mitochondria and apicoplast has also been observed and may be
229 important for organelle biogenesis^{38,39}.

230 To clarify its localization and function, we constructed a *P. falciparum* strain in
231 which the endogenous *PfFtsH1* locus was modified with a C-terminal FLAG epitope and
232 3' UTR tetR-DOZI-binding aptamer sequences for regulated expression³⁰. We first
233 sought to localize *PfFtsH1* with the C-terminal FLAG epitope. However only the FLAG-
234 tagged Cas9 expressed in this strain was detected with no visible band corresponding to
235 the size of *PfFtsH1*, consistent with the previous report that the C-terminus of the protein
236 is cleaved (Extended Data Fig. 5a). *TgFtsH1* was proposed to be C-terminally cleaved in
237 the apicoplast⁴⁰. We hypothesized that if cleavage of *PfFtsH1* is a result of apicoplast
238 localization, then IPP-rescued parasites lacking an apicoplast would retain an intact
239 *PfFtsH1*-FLAG. Indeed, *PfFtsH1*-FLAG was detected in these apicoplast-minus
240 parasites, indicating that C-terminal cleavage of *PfFtsH1* is dependent on the apicoplast
241 (Extended Data Fig. 5). This evidence strongly suggests that *PfFtsH1* traffics to the
242 apicoplast, as has been shown for *TgFtsH1*.

243

244 **Knockdown of *PfFtsH1* disrupts apicoplast biogenesis**

245 Using the endogenously tagged and regulated *PfFtsH1* strain, we determined
246 whether *PfFtsH1* is essential for apicoplast biogenesis. As expected, *PfFtsH1* expression
247 was down-regulated when the tetR-DOZI repressor bound the aptamer sequences, and
248 restored when anhydrotetracycline, which disrupts this interaction, was added (Fig. 3a,
249 Extended Data 5B)³⁰. Upon downregulation of *PfFtsH1*, we observed a nearly 4-fold
250 decrease in parasitemia after 3 replication cycles, compared to parasites expressing
251 normal levels of *PfFtsH1* (Fig 3b, Extended Data Fig. 6a). This growth defect observed
252 over multiple replication cycles reflected the slower kinetics of genetic regulation
253 (compared to chemical inhibition) and partial knockdown, which has been reported using
254 this regulation system (personal communication, Prof. Dan Goldberg). Significantly,
255 growth of *PfFtsH1* knockdown parasites was restored by addition of IPP (Fig 3b,
256 Extended Data 6a). Finally, we confirmed that loss of *PfFtsH1* led to apicoplast loss.
257 Using qPCR, we observed a steady decrease in the apicoplast:nuclear genome ratio upon
258 knockdown of *PfFtsH1* under IPP rescue compared to control parasites, consistent with
259 loss of the apicoplast⁸ (Fig. 3c). These results demonstrate that *PfFtsH1* is required for
260 apicoplast biogenesis and is the first molecular player in apicoplast biogenesis identified
261 in an unbiased screen.

262

263 **Knockdown of *FtsH1* results in specific hypersensitivity to actinonin**

264 Because knockdown of *PfFtsH1* phenocopies the apicoplast biogenesis defect of
265 actinonin, we sought to determine whether actinonin functionally inhibits *PfFtsH1*.
266 Although we identified an actinonin-resistant mutation in *TgFtsH1* encoding an N805S
267 variant, this residue is not conserved between the *P. falciparum* and *T. gondii* homologs
268 and does not allow the same resistant mutation to be tested³⁵. As an alternative, we down-
269 regulated *PfFtsH1* expression and observed a >50-fold decrease in the actinonin EC₅₀
270 compared to control parasites (Fig. 3d). To ensure that the decrease in *PfFtsH1* did not
271 cause confounding effects, growth inhibition was measured over a single replication
272 cycle during which *PfFtsH1* downregulation did not significantly affect parasite growth
273 (Fig. 3b, Extended Data Fig. 6b). Thus reduced levels of *PfFtsH1* caused hypersensitivity
274 to actinonin, analogous to drug-induced haploinsufficiency which is commonly used in
275 yeast to identify drug mechanism-of-action^{41,42}. Importantly, *PfFtsH1* downregulation did

276 not alter the EC₅₀ of fosmidomycin, which blocks apicoplast metabolism, or
277 chloramphenicol, which causes delayed biogenesis defects. These negative controls
278 indicate that the functional interaction of *PfFtsH1* with actinonin is specific and is not
279 observed with other inhibitors that disrupt apicoplast metabolism or biogenesis (Extended
280 Data Fig. 6c-d). This specific and strong chemical-genetic interaction indicates that
281 *PfFtsH1* is required for actinonin's mechanism-of-action.

282

283 **Actinonin inhibits *PfFtsH1* activity *in vitro***

284 After our results revealed a specific and biologically relevant functional
285 interaction between actinonin and *PfFtsH1* in intact parasites, we sought to determine
286 whether actinonin directly inhibits *PfFtsH1* enzymatic activity *in vitro*. *PfFtsH1*₉₁₋₆₁₂
287 lacking its transmembrane domain was expressed as a soluble fusion protein and purified
288 using tandem affinity tags (Figure 4a; Extended figure 7a). As expected, the purified
289 enzyme showed ATPase and protease activity (Extended Data Fig. 7a; Figure 4b-c).
290 Specific mutations reported to inactivate the ATPase (E249Q) or protease (D493A)
291 domains in other AAA+ proteases^{43,44} abolished these respective activities in the *PfFtsH1*
292 construct (Figure 4a-c)^{43,44}. Notably, actinonin inhibited *PfFtsH1* protease activity with
293 an IC₅₀ ≤ 0.6 μM (Figure 4d) (sensitivity limitations of the assay precluded a more
294 accurate number). The metal-binding hydroxamate group of actinonin is known to be
295 very important for inhibition of peptide deformylase²⁵. To determine the contribution of
296 the hydroxamate group to the inhibition of *PfFtsH1*, we tested its inhibition by
297 actinamide, an analog in which the hydroxamate is replaced with an amide. Indeed,
298 actinamide was at least 10-fold less potent against *PfFtsH1* (IC₅₀=7.3 μM; Fig. 4e)²⁷. The
299 decreased enzymatic inhibition correlated with a substantial decrease in parasite growth
300 inhibition compared to actinonin, although growth inhibition by actinamide was still
301 dependent on *PfFtsH1* levels (Extended Data Fig 7b, Fig. 4d). Hence, the direct inhibition
302 of *PfFtsH1* enzymatic activity by actinonin demonstrates that *PfFtsH1* is its target in *P.*
303 *falciparum*.

304

305 **Discussion**

306 We identified actinonin as a first-in-class antimalarial based on its distinct
307 apicoplast inhibition phenotype compared to known inhibitors. Because the phenotypic
308 screen and the mechanism-of-action elucidation were unbiased, the identification of
309 apicomplexan FtsH1 as actinonin's molecular target was surprising in a number of ways.
310 First, the actinonin target in bacteria and mammalian mitochondria is PDF, and *PfPDF*
311 was presumed to be the target in *Plasmodium* parasites^{25,27}. However, our functional
312 assays did not support this hypothesis. Identification of antimalarial drug targets based on
313 homology with known drug targets in distantly related organisms can be misleading. For
314 example, the misidentification of fatty acid enzyme *PfFabI* as the target of triclosan,
315 based on its inhibition of bacterial homologs, led to failed drug development programs
316 when fatty acid biosynthesis was later shown to be dispensable in blood-stage
317 *Plasmodium*^{5,6,45}.

318 Second, though *P. falciparum* and *T. gondii* share conserved apicoplast biogenesis
319 pathways, it was uncertain whether *T. gondii*'s tractable culture system and genetics
320 could be leveraged to identify the actinonin target in *P. falciparum*. Fortunately,
321 actinonin caused apicoplast biogenesis defects in both *P. falciparum* and *T. gondii*

322 supporting a common mechanism-of-action. Specifically, actinonin-treated *P. falciparum*
323 formed “apicoplast-minus parasites” with IPP rescue while *T. gondii* formed them
324 spontaneously^{8,46}. Importantly we show that, unlike in *T. gondii*, disruption of apicoplast
325 biogenesis does not necessarily lead to delayed death in *P. falciparum*. Based on our
326 experience, drug resistance selection in *T. gondii* to aid in elucidating antimalarial
327 mechanism-of-action, where resistant *P. falciparum* cannot be selected, is a powerful
328 approach. The evidence for FtsH1 as the common actinonin target in these two related
329 organisms greatly strengthens the target identification.

330 Third, we identified an actinonin-resistant mutation in *TgFtsH1* but, since *P.*
331 *falciparum* contains 3 FtsH homologs, it was not initially clear which of them was the
332 *TgFtsH1* ortholog. Almost all eukaryotes contain at least two FtsH homologs located in
333 the mitochondrial inner membrane: The i-AAA has a single transmembrane domain with
334 catalytic domains facing the intermembrane space, while the m-AAA has two
335 transmembrane domains and faces the matrix⁴⁷. PF3D7_1119600 is the only homolog
336 predicted to have two transmembrane domains and phylogenetically clusters with human
337 and yeast m-AAA³⁷. Of the two homologs with a single transmembrane domain,
338 PF3D7_1464900 is more closely related to mitochondrial i-AAA from human and yeast,
339 leaving *PfFtsH1* as the apparent ortholog of *TgFtsH1*³⁷. However this pairing
340 contradicted localization studies assigning *TgFtsH1* to the apicoplast and *PfFtsH1* to the
341 mitochondria^{35,37}. *TgFtsH1* was shown to undergo C-terminal processing associated with
342 its trafficking to the apicoplast⁴⁰. Similarly, we showed that *PfFtsH1* undergoes C-
343 terminal processing dependent on the presence of the apicoplast. This shared functional
344 phenotype strongly suggests that *PfFtsH1* also traffics to the apicoplast. Therefore, the
345 most parsimonious assignment for the three *Plasmodium* FtsH homologs is
346 PF3D7_1119600 and PF3D7_1464900 are mitochondrial and *PfFtsH1* is in the
347 apicoplast. Unfortunately, we were unable to generate endogenously-tagged knockdown
348 strains of either PF3D7_1119600 or PF3D7_1464900 to perform localization and
349 functional studies (see Methods).

350 Finally, there are multiple potential metalloproteases in *P. falciparum* and *T.*
351 *gondii* that may be inhibited by actinonin. However, our evidence demonstrates that the
352 primary target of actinonin in these parasites, associated with its disruption of apicoplast
353 biogenesis, is FtsH1. Using IPP rescue to gauge apicoplast specificity, we assayed for
354 secondary targets in *P. falciparum* and detected a non-IPP rescuable target at an actinonin
355 concentration 20-fold higher than that for its apicoplast-specific target (Extended figure
356 1A). Similarly, in *T. gondii*, the loss of “delayed death” growth inhibition (and its
357 associated formation of apicoplast-minus parasites) signified actinonin’s inhibition of a
358 secondary target at a concentration 3.5-fold greater than its specific inhibition of *TgFtsH1*
359 (Extended figure 4b). Moreover, actinonin preferentially targets metalloproteases from
360 MEROPS clan MA composed of structurally homologous proteins with a conserved
361 metal-binding HEXXH motif and catalytic Glu⁴⁸. Out of six metalloproteases predicted to
362 localize to the apicoplast, only FtsH and PDF are in clan MA^{26,37,49–52}. Curiously, FtsH1
363 is the first FtsH homolog shown to be inhibited by actinonin or any small molecule.

364 Overall, we conclude that apicomplexan FtsH1 is the target of actinonin based on
365 1) an actinonin-resistant N805 variant in *TgFtsH1*, 2) disruption of apicoplast biogenesis
366 upon *PfFtsH1* knockdown, phenocopying actinonin’s biogenesis defect, 3) specific
367 actinonin-induced sensitization to *PfFtsH1* knockdown, and 4) *in vitro* inhibition of

368 *Pf*FtsH1 protease activity by actinonin. The unpredicted outcome underscores the power
369 of unbiased screens to uncover novel drug targets in unique but poorly characterized
370 cellular pathways. As the first screen for drug targets in essential apicoplast biogenesis
371 pathways, the approach highlighted in our study provides a framework for similar screens
372 in the future.

373 Our finding also presents an exciting opportunity for antimalarial drug discovery.
374 FtsH1 inhibitors will have significant advantages over existing antimalarials that target
375 apicoplast metabolism or gene expression. Whereas metabolic needs vary throughout the
376 parasite lifecycle and even between the same stage of different *Plasmodium* species^{53,54},
377 apicoplast biogenesis is required at every proliferative stage of the parasite lifecycle and
378 is highly conserved among apicomplexan parasites. For example, apicoplast translation
379 inhibitors have broad clinical application as malaria prophylaxis targeting liver-stage
380 *Plasmodium* spp and as a partner drug, in combination with faster-acting compounds, for
381 acute parasitic diseases targeting blood-stage *Plasmodium* spp, *Toxoplasma gondii*, and
382 *Babesia* spp. In fact, the utility of these antibiotics as antiparasitics would be greater if
383 not for their slow activity. Inhibition of FtsH1 retains all the benefits of targeting
384 apicoplast biogenesis with no delay in the onset-of-action. Moreover, our inability to
385 select actinonin-resistant *Plasmodium* contrasts with the ready selection of *in vitro*
386 resistance against antibiotics and MEP inhibitors and indicates a lower likelihood of
387 clinical resistance to FtsH1 inhibitors^{21,55-57}. Finally, several clinical lead candidates
388 based on the actinonin scaffold (e.g. GSK1322322, LBM-415, BB83698) have advanced
389 into human clinical trials as bacterial PDF inhibitors, setting precedence that actinonin
390 analogs can meet strong clinical entry criteria including selectivity for *Pf*FtsH1 over
391 human metalloproteases⁵⁸. Taken together, FtsH1 inhibitors have potential for rapid
392 onset, multi-stage efficacy against multiple parasitic infections, and minimal clinical
393 resistance and routes to identifying a clinical lead candidate are readily accessible.

394 To pursue this goal, optimization of actinonin's antimalarial activity and drug
395 properties to identify a lead candidate suitable for testing in mouse malarial models will
396 be imperative. Both the *Pf*FtsH1 activity assay and *P. falciparum* FtsH1 knockdown
397 strain reported in our study may be adapted for high-throughput screening of actinonin
398 derivatives with increased potency and specificity. Structures of *Pf*FtsH1 +/- actinonin
399 bound will aid in design of analogs. Importantly, optimization of *Pf*FtsH1 inhibitors will
400 benefit enormously from a "piggyback" strategy to access compound libraries,
401 counterscreens for off-target activity against human metalloproteases, and knowledge
402 about drug properties of actinonin-based scaffolds, which have already been established
403 for bacterial PDF inhibitor programs⁵⁸.

404 Finally, apicomplexan FtsH1 is the first novel molecular player in apicoplast
405 biogenesis identified in an unbiased screen. Acquired by secondary endosymbiosis of an
406 alga, the apicoplast is evolutionarily distinct. FtsH1's role in organelle biogenesis is not
407 conserved in homologs found in mitochondria or primary chloroplasts and likely
408 represents a novel pathway unique to secondary endosymbionts in this parasite
409 lineage^{17,32,59,60}. FtsH homologs have broad substrate specificity to perform general
410 degradation of misfolded membrane proteins⁴⁷. However they have also been shown to
411 catalyze the proteolysis of native cytosolic proteins under specific conditions critical for
412 cellular regulation⁶¹. For example, the essential function of *E. coli* FtsH is its regulated
413 proteolysis of LpxC, the key enzyme in lipopolysaccharide biosynthesis⁶². In *Bacillus*

414 *subtilis*, FtsH-dependent degradation of SpoIVFA regulates spore differentiation⁶³.
415 Similarly, *EcFtsH* degrades a CII transcription factor required for the lysis-lysogeny
416 decision by phage lambda⁶⁴. Based on these regulatory functions of bacterial FtsH
417 homologs, we propose that apicomplexan FtsH1 regulates the proteolysis of key
418 apicoplast membrane protein(s) during parasite replication. Identification of these
419 substrates will be critical to understanding its molecular mechanism in apicoplast
420 biogenesis. FtsH1 offers a rare foothold into a novel apicoplast biogenesis pathway
421 evolved from secondary endosymbiosis and will yield deeper insight into the molecular
422 mechanisms of eukaryogenesis.

423

424 **References**

425

426 1. McFadden, G. I., Reith, M. E., Munholland, J. & Lang-Unnasch, N. Plastid in human

427 parasites. *Nature* **381**, 482 (1996).

428 2. Köhler, S. *et al.* A plastid of probable green algal origin in Apicomplexan

429 parasites. *Science* **275**, 1485–1489 (1997).

430 3. Jomaa, H. *et al.* Inhibitors of the nonmevalonate pathway of isoprenoid

431 biosynthesis as antimalarial drugs. *Science* **285**, 1573–1576 (1999).

432 4. Mazumdar, J., H Wilson, E., Masek, K., A Hunter, C. & Striepen, B. Apicoplast fatty

433 acid synthesis is essential for organelle biogenesis and parasite survival in

434 *Toxoplasma gondii*. *Proc. Natl. Acad. Sci. U. S. A.* **103**, 13192–13197 (2006).

435 5. Vaughan, A. M. *et al.* Type II fatty acid synthesis is essential only for malaria

436 parasite late liver stage development. *Cell. Microbiol.* **11**, 506–520 (2009).

437 6. Yu, M. *et al.* The Fatty Acid Biosynthesis Enzyme FabI Plays a Key Role In the

438 Development of Liver Stage Malarial Parasites. *Cell Host Microbe* **4**, 567–578

439 (2008).

440 7. Nair, S. C. *et al.* Apicoplast isoprenoid precursor synthesis and the molecular

441 basis of fosmidomycin resistance in *Toxoplasma gondii*. *J. Exp. Med.* (2011).

442 doi:10.1084/jem.20110039

- 443 8. Yeh, E. & DeRisi, J. L. Chemical Rescue of Malaria Parasites Lacking an Apicoplast
444 Defines Organelle Function in Blood-Stage *Plasmodium falciparum*. *PLoS Biol* **9**,
445 e1001138 (2011).
- 446 9. Ke, H. *et al.* The heme biosynthesis pathway is essential for *Plasmodium*
447 *falciparum* development in mosquito stage but not in blood stages. *J. Biol. Chem.*
448 **289**, 34827–34837 (2014).
- 449 10. Fichera, M. E. & Roos, D. S. A plastid organelle as a drug target in apicomplexan
450 parasites. *Nature* **390**, 407–409 (1997).
- 451 11. Dahl, E. L. *et al.* Tetracyclines specifically target the apicoplast of the malaria
452 parasite *Plasmodium falciparum*. *Antimicrob. Agents Chemother.* **50**, 3124–3131
453 (2006).
- 454 12. Geary, T. G. & Jensen, J. B. Effects of antibiotics on *Plasmodium falciparum* in
455 *vitro*. *Am. J. Trop. Med. Hyg.* **32**, 221–225 (1983).
- 456 13. Oyakhirome, S. *et al.* Randomized controlled trial of fosmidomycin-clindamycin
457 versus sulfadoxine-pyrimethamine in the treatment of *Plasmodium falciparum*
458 malaria. *Antimicrob. Agents Chemother.* **51**, 1869–1871 (2007).
- 459 14. Lanaspá, M. *et al.* Inadequate Efficacy of a New Formulation of Fosmidomycin-
460 Clindamycin Combination in Mozambican Children Less than Three Years Old
461 with Uncomplicated *Plasmodium falciparum* Malaria. *Antimicrob. Agents*
462 *Chemother.* **56**, 2923–2928 (2012).
- 463 15. Guggisberg, A. M. *et al.* Whole-Genome Sequencing to Evaluate the Resistance
464 Landscape Following Antimalarial Treatment Failure With Fosmidomycin-
465 Clindamycin. *J. Infect. Dis.* **214**, 1085–1091 (2016).

- 466 16. Waller, R. F. *et al.* Nuclear-encoded proteins target to the plastid in *Toxoplasma*
467 *gondii* and *Plasmodium falciparum*. *Proc. Natl. Acad. Sci.* **95**, 12352–12357
468 (1998).
- 469 17. Vaishnava, S. & Striepen, B. The cell biology of secondary endosymbiosis--how
470 parasites build, divide and segregate the apicoplast. *Mol. Microbiol.* **61**, 1380–
471 1387 (2006).
- 472 18. Spangenberg, T. *et al.* The Open Access Malaria Box: A Drug Discovery Catalyst
473 for Neglected Diseases. *PLoS ONE* **8**, e62906 (2013).
- 474 19. Wiesner, J., Sanderbrand, S., Altincicek, B., Beck, E. & Jomaa, H. Seeking new
475 targets for antiparasitic agents. *Trends Parasitol.* **17**, 7–8 (2001).
- 476 20. Dahl, E. L. & Rosenthal, P. J. Multiple Antibiotics Exert Delayed Effects against the
477 *Plasmodium falciparum* Apicoplast. *Antimicrob Agents Chemother* **51**, 3485–
478 3490 (2007).
- 479 21. Wu, W. *et al.* A chemical rescue screen identifies a *Plasmodium falciparum*
480 apicoplast inhibitor targeting MEP isoprenoid precursor biosynthesis.
481 *Antimicrob. Agents Chemother.* AAC.03342-14 (2014). doi:10.1128/AAC.03342-
482 14
- 483 22. Gisselberg, J. E., Herrera, Z., Orchard, L., Llinas, M. & Yeh, E. A Specific Non-
484 Bisphosphonate Inhibitor Of The Bifunctional Farnesyl/Geranylgeranyl
485 Diphosphate Synthase In Malaria Parasites. *bioRxiv* 134338 (2017).
486 doi:10.1101/134338
- 487 23. Gordon, J. J., Kelly, B. K. & Miller, G. A. Actinonin: an antibiotic substance
488 produced by an actinomycete. *Nature* **195**, 701–702 (1962).

- 489 24. Goodman, C. D. & McFadden, G. I. Ycf93 (Orf105), a small apicoplast-encoded
490 membrane protein in the relict plastid of the malaria parasite *Plasmodium*
491 *falciparum* that is conserved in Apicomplexa. *PLoS One* **9**, e91178 (2014).
- 492 25. Chen, D. Z. *et al.* Actinonin, a naturally occurring antibacterial agent, is a potent
493 deformylase inhibitor. *Biochemistry (Mosc.)* **39**, 1256–1262 (2000).
- 494 26. Bracchi-Ricard, V. *et al.* Characterization of an eukaryotic peptide deformylase
495 from *Plasmodium falciparum*. *Arch. Biochem. Biophys.* **396**, 162–170 (2001).
- 496 27. Lee, M. D. *et al.* Human mitochondrial peptide deformylase, a new anticancer
497 target of actinonin-based antibiotics. *J. Clin. Invest.* **114**, 1107–1116 (2004).
- 498 28. Kumar, A. *et al.* Crystals of peptide deformylase from *Plasmodium falciparum*
499 reveal critical characteristics of the active site for drug design. *Struct. Lond. Engl.*
500 *1993* **10**, 357–367 (2002).
- 501 29. Margolis, P. S. *et al.* Peptide Deformylase in *Staphylococcus aureus*: Resistance to
502 Inhibition Is Mediated by Mutations in the Formyltransferase Gene. *Antimicrob.*
503 *Agents Chemother.* **44**, 1825–1831 (2000).
- 504 30. Ganesan, S. M., Falla, A., Goldfless, S. J., Nasamu, A. S. & Niles, J. C. Synthetic RNA-
505 protein modules integrated with native translation mechanisms to control gene
506 expression in malaria parasites. *Nat. Commun.* **7**, 10727 (2016).
- 507 31. Richter, U. *et al.* A Mitochondrial Ribosomal and RNA Decay Pathway Blocks Cell
508 Proliferation. *Curr. Biol.* **23**, 535–541 (2013).
- 509 32. van Dooren, G. G. *et al.* A novel dynamin-related protein has been recruited for
510 apicoplast fission in *Toxoplasma gondii*. *Curr. Biol. CB* **19**, 267–276 (2009).

- 511 33. Jacot, D., Daher, W. & Soldati-Favre, D. Toxoplasma gondii myosin F, an essential
512 motor for centrosomes positioning and apicoplast inheritance. *EMBO J.* **32**,
513 1702–1716 (2013).
- 514 34. Lévêque, M. F. *et al.* Autophagy-Related Protein ATG8 Has a Noncanonical
515 Function for Apicoplast Inheritance in Toxoplasma gondii. *mBio* **6**, e01446-1415
516 (2015).
- 517 35. Karnataki, A., Derocher, A. E., Coppens, I., Feagin, J. E. & Parsons, M. A membrane
518 protease is targeted to the relict plastid of toxoplasma via an internal signal
519 sequence. *Traffic Cph. Den.* **8**, 1543–1553 (2007).
- 520 36. Ganji, R. J. *et al.* Structural basis for the inhibition of M1 family aminopeptidases
521 by the natural product actinonin: Crystal structure in complex with E. coli
522 aminopeptidase N. *Protein Sci. Publ. Protein Soc.* **24**, 823–831 (2015).
- 523 37. Tanveer, A. *et al.* An FtsH protease is recruited to the mitochondrion of
524 Plasmodium falciparum. *PloS One* **8**, e74408 (2013).
- 525 38. van Dooren, G. G. *et al.* Development of the endoplasmic reticulum,
526 mitochondrion and apicoplast during the asexual life cycle of Plasmodium
527 falciparum. *Mol. Microbiol.* **57**, 405–419 (2005).
- 528 39. Stanway, R. R. *et al.* Organelle segregation into Plasmodium liver stage
529 merozoites. *Cell. Microbiol.* **13**, 1768–1782 (2011).
- 530 40. Sequential processing of the Toxoplasma apicoplast membrane protein FtsH1 in
531 topologically distinct domains during intracellular trafficking. Available at:
532 <http://www.ncbi.nlm.nih.gov/pmc/articles/PMC2817949/>. (Accessed: 22nd
533 June 2016)

- 534 41. Giaever, G. *et al.* Genomic profiling of drug sensitivities via induced
535 haploinsufficiency. *Nat. Genet.* **21**, 278–283 (1999).
- 536 42. Baetz, K. *et al.* Yeast genome-wide drug-induced haploinsufficiency screen to
537 determine drug mode of action. *Proc. Natl. Acad. Sci. U. S. A.* **101**, 4525–4530
538 (2004).
- 539 43. Hersch, G. L., Burton, R. E., Bolon, D. N., Baker, T. A. & Sauer, R. T. Asymmetric
540 interactions of ATP with the AAA+ ClpX6 unfoldase: allosteric control of a
541 protein machine. *Cell* **121**, 1017–1027 (2005).
- 542 44. Bieniossek, C. *et al.* The molecular architecture of the metalloprotease FtsH.
543 *Proc. Natl. Acad. Sci. U. S. A.* **103**, 3066–3071 (2006).
- 544 45. Surolia, N. & Surolia, A. Triclosan offers protection against blood stages of
545 malaria by inhibiting enoyl-ACP reductase of *Plasmodium falciparum*. *Nat. Med.*
546 **7**, 167–173 (2001).
- 547 46. He, C. Y. *et al.* A plastid segregation defect in the protozoan parasite *Toxoplasma*
548 *gondii*. *EMBO J* **20**, 330–339 (2001).
- 549 47. Janska, H., Kwasniak, M. & Szczepanowska, J. Protein quality control in
550 organelles — AAA/FtsH story. *Biochim. Biophys. Acta BBA - Mol. Cell Res.* **1833**,
551 381–387 (2013).
- 552 48. MEROPS - the Peptidase Database. Available at: [http://merops.sanger.ac.uk/cgi-](http://merops.sanger.ac.uk/cgi-bin/smi_summary?mid=J16.404)
553 [bin/smi_summary?mid=J16.404](http://merops.sanger.ac.uk/cgi-bin/smi_summary?mid=J16.404). (Accessed: 10th May 2017)
- 554 49. van Dooren, G. G., Su, V., D’Ombrain, M. C. & McFadden, G. I. Processing of an
555 Apicoplast Leader Sequence in *Plasmodium falciparum* and the Identification of a
556 Putative Leader Cleavage Enzyme. *J. Biol. Chem.* **277**, 23612–23619 (2002).

- 557 50. Mallari, J. P., Oksman, A., Vaupel, B. & Goldberg, D. E. Kinase-associated
558 endopeptidase 1 (Kae1) participates in an atypical ribosome-associated complex
559 in the apicoplast of *Plasmodium falciparum*. *J. Biol. Chem.* **289**, 30025–30039
560 (2014).
- 561 51. Ponpuak, M. *et al.* A role for falcilysin in transit peptide degradation in the
562 *Plasmodium falciparum* apicoplast. *Mol. Microbiol.* **63**, 314–334 (2007).
- 563 52. Chen, X. *et al.* Inhibitors of *Plasmodium falciparum* methionine aminopeptidase
564 1b possess antimalarial activity. *Proc. Natl. Acad. Sci. U. S. A.* **103**, 14548–14553
565 (2006).
- 566 53. Srivastava, A. *et al.* Stage-Specific Changes in *Plasmodium* Metabolism Required
567 for Differentiation and Adaptation to Different Host and Vector Environments.
568 *PLoS Pathog.* **12**, e1006094 (2016).
- 569 54. Shears, M. J., Botté, C. Y. & McFadden, G. I. Fatty acid metabolism in the
570 *Plasmodium* apicoplast: Drugs, doubts and knockouts. *Mol. Biochem. Parasitol.*
571 **199**, 34–50 (2015).
- 572 55. Dharia, N. V. *et al.* Use of high-density tiling microarrays to identify mutations
573 globally and elucidate mechanisms of drug resistance in *Plasmodium falciparum*.
574 *Genome Biol.* **10**, R21 (2009).
- 575 56. Guggisberg, A. M. *et al.* A sugar phosphatase regulates the methylerythritol
576 phosphate (MEP) pathway in malaria parasites. *Nat. Commun.* **5**, 4467 (2014).
- 577 57. Sidhu, A. B. S. *et al.* In vitro efficacy, resistance selection, and structural modeling
578 studies implicate the malarial parasite apicoplast as the target of azithromycin. *J.*
579 *Biol. Chem.* **282**, 2494–2504 (2007).

- 580 58. Sangshetti, J. N., Khan, F. A. K. & Shinde, D. B. Peptide deformylase: a new target
581 in antibacterial, antimalarial and anticancer drug discovery. *Curr. Med. Chem.* **22**,
582 214–236 (2015).
- 583 59. Moore, R. B. *et al.* A photosynthetic alveolate closely related to apicomplexan
584 parasites. *Nature* **451**, 959–963 (2008).
- 585 60. Spork, S. *et al.* An Unusual ERAD-Like Complex Is Targeted to the Apicoplast of
586 *Plasmodium falciparum*. *Eukaryot. Cell* **8**, 1134–1145 (2009).
- 587 61. Bittner, L.-M., Arends, J. & Narberhaus, F. When, how and why? Regulated
588 proteolysis by the essential FtsH protease in *Escherichia coli*. *Biol. Chem.* **398**,
589 625–635 (2017).
- 590 62. Ogura, T. *et al.* Balanced biosynthesis of major membrane components through
591 regulated degradation of the committed enzyme of lipid A biosynthesis by the
592 AAA protease FtsH (HflB) in *Escherichia coli*. *Mol. Microbiol.* **31**, 833–844
593 (1999).
- 594 63. Rudner, D. Z. & Losick, R. A sporulation membrane protein tethers the pro- σ K
595 processing enzyme to its inhibitor and dictates its subcellular localization. *Genes*
596 *Dev.* **16**, 1007–1018 (2002).
- 597 64. Shotland, Y. *et al.* Proteolysis of the phage lambda CII regulatory protein by FtsH
598 (HflB) of *Escherichia coli*. *Mol. Microbiol.* **24**, 1303–1310 (1997).

599

600 **Methods**

601 **Chemicals**

602 Fosmidomycin was purchased from Santa Cruz Biotechnology and 10mM aliquots were
603 prepared in water. Chloramphenicol was purchased from Sigma Aldrich and 50mM
604 aliquots were prepared in 100% ethanol. Actinonin was purchased from Sigma Aldrich
605 and 25mM aliquots were prepared in 100% ethanol. Anhydrotetracycline was purchased
606 from Sigma and 2.5mM aliquots prepared in 100% ethanol and used at a final

607 concentration of 0.5uM. Actinamide was a gift from Drs. David Scheinberg and Ouathek
608 Ouerfelli and 25mM aliquots were prepared in 100% ethanol.

609
610 Enoxacin, ciprofloxacin, levofloxacin, norfloxacin, novobiocin, coumeramycin,
611 mericitabine, 2’deoxy-2-F-cytidine, gemcitabine, ADEP1a, beta-lactone 4, beta-lactone
612 7, and rifampin were acquired and solubilized as noted in Supplementary Table 1.

613
614 Isopentenyl pyrophosphate (IPP) was purchased from Isoprenoids LC and stored at 2
615 mg/mL in 70% methanol, 30% 10mM ammonium hydroxide at -80C. To prevent
616 methanol toxicity, aliquots of IPP were dried in the speed vacuum centrifuge before
617 adding to cultures. All drugs were stored at -20C and resuspended just prior to use.

618 619 ***Plasmodium falciparum* culture and transfections**

620 *P. falciparum* D10 (MRA-201), and D10 ACP_L-GFP (MRA-568) were obtained from
621 MR4. *P. falciparum* NF54^{attB} was a gift from David Fidock (Columbia University). NF54
622 ^{attB} strain constitutively expressing Cas9 and T7 Polymerase, generated previously⁶³, was
623 used in this study. Parasites were maintained in human erythrocytes (2% hematocrit) in
624 RPMI 1640 media supplemented with 0.25% Albumax II (GIBCO Life Technologies), 2
625 g/L sodium bicarbonate, 0.1 mM hypoxanthine, 25 mM HEPES (pH 7.4), 50 µg/L
626 gentamycin, and 0.4% glucose at 37°C, 5% O₂, and 5% CO₂. All cell lines tested
627 negative for mycoplasma contamination during routine checks.

628
629 Parasites were transfected using methods already published³⁰. Briefly, we used 50 ug of
630 plasmid per 200 uL packed red blood cells (RBCs) adjusted to 50% hematocrit. We used
631 a Bio-Rad Gene Pulser II to preload uninfected RBCs using eight square-wave pulses of
632 365 V for 1 ms, separated by 100 ms. Preloaded RBCs were resealed for 1 hour at 37C
633 and washed twice in RPMI to remove lysed cells. Schizont stage parasites at 0.5%
634 parasitemia were then allowed to invade half of the preloaded RBCs during two
635 sequential reinvasions. Media was changed daily for the first 12 days and every other day
636 thereafter. Parasites were split 1:1 into fresh blood every 4 days until parasites were
637 visible by Giemsa smear. To select for integration of the pFtsH1 into *P. falciparum*
638 NF54^{attB-pPFCRISPR} parasites, transfected parasites were maintained in media containing 5
639 nM WR99210 and 0.5 uM anhydrotetracycline (Sigma) and then selected with 2.5 mg/l
640 Blastocidin S (Sigma) beginning 4 days after transfection.

641 642 ***Toxoplasma gondii* culture and transfection**

643 *T. gondii* RH and *T. gondii* RH $\Delta ku80\Delta hxpprt$ strains were a gift from Matthew Bogyo
644 (Stanford University) and maintained by passage through confluent monolayers of human
645 foreskin fibroblasts (HFFs) host cells. HFFs were cultured in DMEM (Invitrogen)
646 supplemented with 10% FBS (Fetal Plex Animal Serum from Gemini), 2mM L-
647 glutamine (Gemini), and 100 ug penicillin and 100 ug streptomycin per mL (Gibco Life
648 Technologies), maintained at 37 C and 5% CO₂. Parasites were harvested for assays by
649 syringe lysis of infected HFF monolayers.

650
651 For transfection of *T. gondii* $\Delta ku80\Delta hxpprt$, 15ug of the pTgCRISPR plasmid⁶⁵ was
652 combined with 3 ug of the pFtsH1N805S or pFtsH1WT that had been linearized by NotI

653 digestion. Approximately 10^7 parasites were released from host cells using syringe lysis
654 and washed into 400 μ L of cytomix containing both plasmids. Parasites were
655 eletroporated (BTX Electro Cell Manipulator 600) with 1.2-1.4 kV, 2.5kV/resistance, R2
656 (24 ohm) and then allowed to recover in the cuvette at room temperature for 10 mins
657 before adding to host cells. After 24 hours, media containing 25 μ g/mL mycophenolic
658 acid (Sigma) and 50 μ g/mL xanthine (Sigma) was added to select for transfectants. After
659 a week, plaques were observed and single clones were isolated using limiting dilution.

660

661 ***Toxoplasma gondii* genome sequencing and SNP identification**

662 Actinonin resistant and susceptible *T. gondii* were grown on 15 cm dishes containing
663 confluent HFF monolayers until spontaneous lysis of the monolayer was achieved.
664 Released parasites were collected and filtered through 5 micrometer syringe filters
665 (Millipore) before isolating DNA (Qiagen DNAeasy Blood & Tissue).

666

667 *T. gondii* genomic DNA isolated from either the parental *T. gondii* RH strain
668 (SRR3666219) or any of its derived mutants (SRR3666219, SRR3666222, SRR3666224,
669 SRR3666792, SRR3666794, SRR3666796, SRR3666798, SRR3666799, SRR3666801)
670 was sequenced in an Illumina NextSeq apparatus using 2x150bp reads at an average
671 sequencing depth of 35x. Sequencing reads were quality trimmed and remnants of
672 sequencing adaptors removed with *trimmomatic* (PMID:24695404). Next, reads were
673 mapped to the reference nuclear assembly of the *T. gondii* GT1 strain (ToxoDB v13.0)
674 and the apicoplast genome assembly from the RH strain (NC_001799) with the program
675 *bowtie2* (PMID:25621011). Duplicated aligned reads were removed with *picard tools*
676 (<http://broadinstitute.github.io/picard>) and reads spanning InDels were realigned with
677 GATK (PMID:20644199). Afterwards, allelic variants were called with *samtools mpileup*
678 (PMID:19505943) followed by *bcftools call* with $-p$ set to 0.05 (PMID:26826718).
679 Finally, classification of mutations was performed with *snpEff* (PMID:22728672).

680

681 **Growth inhibition assays**

682 For *P. falciparum* EC₅₀ calculations, growth assays were performed in 96 well plates
683 containing serial dilution of drugs in triplicate. Media was supplemented with 200 μ M
684 IPP as indicated. Growth was initiated with ring-stage parasites (synchronized with 5%
685 sorbitol treatment) at 1% parasitemia and 1% hematocrit. To calculate growth, cultures
686 were incubated for 72h and growth was then terminated by incubation with 1%
687 formaldehyde (Electron Microscopy Services) for 30 minutes at room temperature.
688 Parasitized cells were stained with 50 nM YOYO-1 (Invitrogen) overnight at room
689 temperature and the parasitemia was determined by flow cytometry (BD Accuri C6
690 Sampler). Data were analyzed by BD Accuri C6 Sampler software. *P. falciparum* growth
691 assays measuring the actinonin EC₅₀ were repeated in the laboratory > 10 times for WT
692 parasites and >3 times upon knockdown of FtsH1.

693

694 For *T. gondii* EC₅₀ calculations, plaque assays were performed in 24 well plates
695 containing confluent HFF monolayers serial dilutions of drugs in duplicate.
696 Approximately 50 parasites were counted using flow cytometry and added to each well.
697 After incubating for 6 days, infected monolayers were washed, fixed with methanol for
698 10 minutes, stained with 2% crystal violet (Sigma) for 30 minutes, and then washed

699 again. Plaques were visualized as non-stained areas. The area of each plaque in a given
700 well was measured and summed using ImageJ as a proxy for growth and normalized to
701 the vehicle only control. *T. gondii* plaque assays measuring the actinonin EC₅₀ were
702 repeated in the laboratory > 2 times for resistant parasites that arose from actinonin
703 selection, > 10 times for WT parasites, and > 3 times for TgFtsH(N805S).

704

705 For measuring the growth inhibition of *P. falciparum* during the time course, 10 uM
706 actinonin, 10 uM fosmidomycin, 30 uM chloramphenicol, 200 uM IPP, and 0.5 uM of
707 anhydrotetracycline was used as necessary. For comparison of growth between different
708 treatment conditions, cultures were carried simultaneously and handled identically with
709 respect to media changes and addition of blood cells. Daily samples were collected and
710 fixed with 1% formaldehyde for 30 minutes at RT. At the end of the time course, all
711 samples were stained with 50 nM YOYO-1 and parasitemia was measured using flow
712 cytometry. All growth curves were plotted using GraphPad Prism. *P. falciparum* time
713 course experiments were repeated in the laboratory > 2 times for WT parasites and > 2
714 times upon knockdown of FtsH1.

715

716 For measuring the growth inhibition of *T. gondii* during the time course, 6-well plates
717 were set up with no drug, 40 uM actinonin, 25 nM clindamycin, and 4 uM
718 pyrimethamine. *T. gondii* was added at a MOI = 3. Every 12 hours, parasites were
719 released from HFFs using syringe lysis and counted using flow cytometry (BD Accuri C6
720 Sampler). After 36 hours, spontaneous lysis of the monolayer was observed and parasites
721 were counted using flow cytometry and then added back to fresh monolayers at MOI = 3
722 in the absence of drug and parasites were counted every 12 hours as before. *T. gondii*
723 time course experiments were repeated in the laboratory > 2 times.

724

725 For measuring growth inhibition using tandem-tomato expression as a proxy for growth,
726 tandem-tomato *T. gondii* were seeded onto a black, clear bottom 96 well plate (Costar
727 3603) at 2000 parasites per well. Parasites were treated at a range of drug concentrations
728 and fluorescence was measured daily in a plate reader (BioTek, Synergy) for 5 days using
729 the bottom read function.

730

731 For co-treatments of *P. falciparum* with actinonin and chloramphenicol, 96 well plates
732 containing ring stage parasites at 1% parasitemia and 1% hematocrit were treated with
733 serial dilutions of both actinonin and chloramphenicol alone and in combination. To
734 determine the effect on growth after one lytic cycle, parasites were fixed at 72h and
735 parasitemia was measured by flow cytometry as above. To determine the effect on
736 growth after two lytic cycles, 75% of the media was exchanged at 72 hours and plates
737 were incubated for an additional 48 hours following fixation and flow cytometry as
738 above. Media was supplemented with 200 uM IPP as a separate control to insure
739 specificity of the drug at the concentrations used. Co-treatments with actinonin and
740 chloramphenicol were performed a single time in the laboratory using three technical
741 replicates.

742

743 **Quantitative Real-Time PCR**

744 Parasites from 1 mL of *P. falciparum* culture at ring stage were isolated by saponin lysis
745 followed by two washes with PBS. DNA was purified using DNAeasy Blood & Tissue
746 (Qiagen). Primers were designed to target genes found on the apicoplast or nuclear
747 genome: *tufA* (apicoplast) 5'-GATATTGATTCAGCTCCAGAAGAAA-3' and *CHT1*
748 (nuclear) 5'-TGTTTCCTTCAACCCCTTTT-3' /5'-TGTTTCCTTCAACCCCTTTT-3'.
749 Reactions contained template DNA, 0.15 uM of each primer, and 1x SYBR Green I
750 Master mix (Roche). qPCR reactions were performed at 56C primer annealing and 65C
751 template extension for 35 cycles on a Applied Biosystem 7900HT system. Relative
752 quantification of target genes was determined⁶⁴. For each time point, the
753 apicoplast:nuclear genome ratio was calculated relative to the appropriate control
754 collected at the same time. The apicoplast:nuclear genome ratio was measured by qPCR
755 > 5 times for WT parasites treated with actinonin and > 2 times upon knockdown of
756 FtsH1.

757

758 **Fluorescence Microscopy**

759 *P. falciparum* D10 ACP(L)-GFP parasites diluted to 0.05% hematocrit were settled on a
760 Lab-Tek II Chambered Coverglass (Thermo Fisher) and incubated in 2 ug/mL Hoescht
761 33342 stain for 15 minutes at 37C. Widefield epifluorescence live cell images were
762 acquired with an Olympus IX70 microscope. The microscope was outfitted with a
763 Deltavision Core system (Applied Precision) using an Olympus x60 1.4NA Plan Apo
764 Lens, a Sedat Quad filter set (Semrock) and a CoolSnap HQ CCD Camera
765 (Photometrics). The microscope was controlled and images were deconvolved via
766 softWoRx 4.1.0 software. ImageJ software was used to analyze resulting images.

767

768 Live microscopy of *T. gondii* RH FNR-RFP parasites⁶⁸ was performing using Lab-Tek II
769 Chambered Coverglasses containing confluent HFF monolayers. Parasites were added at
770 an MOI = 1. After 36 hours of incubation, parasites were incubated with 2 ug/mL of
771 Hoescht for 15 minutes. Widefield epifluorescence live cell images were acquired with a
772 Nikon Eclipse Ti inverted fluorescence microscope with a NA 1.40 oil-immersion
773 objective (Nikon Instruments) and controlled using MicroManager v1.4. An iXon3 888
774 EMCCD camera (Andor) was used for fluorescence imaging and an a Zyla 5.5 sCMOS
775 camera (Andor) was used for phase contrast imaging. ImageJ software was used to
776 analyze the resulting images. ACP-GFP parasites treated with actinonin were imaged > 4
777 different times in the laboratory.

778

779 **Immunoblot**

780 Parasites from 9 mL of *P. falciparum* culture were isolated by saponin lysis, washed with
781 PBS and resuspended in 1 x NuPAGE LDS sample buffer (Invitrogen). Proteins were
782 separated by electrophoresis on 4-12% Bis-Tris gel (Invitrogen) and transferred to a
783 nitrocellulose membrane. After blocking, membranes were probed with 1:2000
784 monoclonal mouse anti-FLAG M2 (Sigma) and 1:10,000 IRDye 680RD goat anti-mouse
785 IgG (LiCor Bioscience) for anti-FtsH1 immunoblots. For anti-PDF immunoblots,
786 membranes were probed with 1:2000 rabbit monoclonal anti-MYC (Cell Signaling
787 Technology 2278S), followed by 1:20,000 rabbit polyclonal anti-PfAldolase (Abcam
788 ab207494) and 1:10,000 donkey anti-rabbit 800 (LiCor Biosciences). Fluorescence
789 antibody-bound proteins were detected with Odyssey Imager (LiCor Biosciences). When

790 antibodies of the same species were used, membranes were probed and imaged
791 sequentially. Immunoblots of FtsH-FLAG and PFD-myc were repeated in the laboratory
792 > 2 times.

793

794 ***Toxoplasma gondii* resistance selection**

795 Approximately 2×10^6 *T. gondii* RH parasites were added to T25s containing a
796 confluent HFF monolayer and allowed to grow for 24 hours. To mutagenize, between
797 500 μ M – 2 mM N-ethyl N-nitrosourea (ENU) diluted in DMSO was added to flasks and
798 incubated for 2 hours at 37 C. Cultures were then washed twice with 10mLs of cold PBS
799 and then released from host cells using syringe lysis. A quarter of the resulting parasites
800 were passaged to T25s containing a fresh monolayer of HFFs. After two passages,
801 parasites were treated with 40 μ M actinonin (the minimum inhibitory concentration of
802 sensitive *T. gondii*). After one passage under actinonin selection, a severe bottleneck was
803 observed. Plaques of resistant parasites could be observed after one week of constant
804 actinonin pressure with periodic media changes. Finally, single clones were isolated
805 using limiting dilution. Actinonin resistance selection was repeated in the laboratory
806 twice.

807

808 ***Plasmodium falciparum* construct generation**

809 The primers used for generating different fragments are listed in the Extended Data Table
810 3. A construct for inducing PfPDF (PF3D7_0907900) expression in *P. falciparum* was
811 generated from the parental pMG96 plasmid. PDF gene was amplified from pUC57-Amp
812 plasmid with the codon optimized PDF gene (PF3D7_0907900) using primers SMG374
813 and SMG375. The amplicon was cloned in PfCAM base plasmid (pMG96), which
814 contains single aptamer at 5'UTR and 10x aptamer at 3'UTR. The restriction sites MScI
815 and BstEII were used for cloning thus encoding PDF containing c-myc tag at the c-
816 terminal end. The transfection was carried out as discussed previously⁶⁹. A construct for
817 regulating expression of FtsH1 (PF3D7_1239700) in *P. falciparum* (pFtsH1) was
818 generated from the parental pSN054, a modified pJazz linear plasmid (Extended Data
819 Table 3). The left homology region was amplified from parasite genomic DNA using
820 primers SMG476 and SMG 477 and was cloned using FseI and AsisI restriction sites.
821 FtsH1 protein coding nucleotides 2348- 2643 were recoded using gene block (IDT) to
822 remove the PAM site. The right homology region was amplified from parasite genomic
823 DNA using primers SMG501 and SMG502. These fragments were cloned using the I-
824 SceI restriction site. Targeting guide RNA was generated by klenow reaction using
825 primers SMG514 and SMG515 and was inserted using the AflII site. All sequences were
826 ligated into the parent plasmid using Gibson assembly. Constructs for regulating
827 PF3D7_1464900 were generated similarly (SMG505 and SMG506 for the right
828 homology region; SMG495 and SMG496 for the left homology region; SMG518 and
829 SMG519 for the gRNA klenow reaction). While this construct could be generated, no
830 parasites emerged after two transfections. Constructs for regulating PF3D7_1119600
831 using primers SMG503 and SMG504 for the right homology region and SMG481 and
832 SMG507 for the left homology region were unable to be generated because of
833 unsuccessful PCR.

834

835 ***Toxoplasma gondii* construct generation**

836 A construct for knocking in the FtsH1_{N805S} allele into the endogenous loci of FtsH1
837 (pFtsHN805S) was generated from the parental pTKO2 vector. Briefly, a ~800 bp
838 sequence upstream of the TGGT1_259260 start codon was amplified as the left
839 homology region (using primers KAJ1 and KAJ2). The FtsH1_{N805S} sequence was then
840 amplified from actinonin resistant cDNA (using primers KAJ3 and KAJ4). The HXGPRT
841 resistance cassette was amplified off of the pTKO2 cassette (using primers KAJ5 and
842 KAJ6). A ~800 bp sequence downstream of the TGGT1_259260 stop codon was
843 amplified as the right homology region (using primers KAJ7 and KAJ8). To insert the
844 right homology region, the pTKO2 plasmid was cut with HindIII and HpaI and the 800
845 bp sequence was inserted using infusion (Clontech). To insert the left homology region
846 and the FtsH1_{N805S} allele, the pTKO2 plasmid containing the downstream homology
847 region was cut with NotI and EcoRI and the two PCR products were inserted also using
848 infusion (Clontech). The resulting colonies were tested using a diagnostic HpaI digest
849 and correct clones were subjected to Sanger sequencing of the inserts. To revert the
850 pFtsHN805S construct to pFtsHWT, we used Q5 mutagenesis (NEB) and primers KAJ9
851 and KAJ10.

852
853 To increase the transfection efficiency and specificity, CRISPR-Cas9 was used to insert a
854 double stranded break at the site of insertion (the endogenous TGGT1_259260 allele).
855 Briefly, pSAG1::Cas9-U6::sgUPRT⁶⁵ was modified to contain a guide sequence specific
856 to a FtsH1 intron using the Q5 mutagenesis kit (NEB) and primers KAJ11 and KAJ12.
857 Sanger sequencing of the guide was used to verify the resulting plasmid.

858

859 **Recombinant *PfFtsH1* expression and purification**

860 His₆-SUMO-*PfFtsH1*₉₁₋₆₁₂-GST was cloned into a pET22-based vector by Gibson
861 assembly⁷¹. Point mutations in this gene were constructed by site-directed mutagenesis.
862 Liquid cultures of T7 Express cells (NEB) harboring these plasmids were grown to log
863 phase, cooled to 20 °C, and induced with 0.5 mM IPTG plus 0.1% benzyl alcohol
864 (Sigma). Cultures were incubated for an additional 3 h at 20 °C before harvesting and
865 freezing. Cell pellets were resuspended in lysis buffer (50 mM HEPES, pH 7.5, 200 mM
866 NaCl, 10% glycerol, 2 mM β-mercaptoethanol [βME], 20 mM imidazole), mixed with
867 lysozyme (1 mg/mL) and Benzonase (Sigma), and lysed by sonication. Cleared lysates
868 were incubated with Ni-NTA resin (G-Biosciences) for 1 h at 4 °C. After extensive
869 washing with lysis buffer, bound proteins were eluted from the resin with lysis buffer
870 plus 300 mM imidazole. The eluent was applied to a GSTrap column (GE Healthcare)
871 and washed with storage buffer (50 mM HEPES, pH 7.5, 200 mM NaCl, 10% glycerol, 2
872 mM βME) before eluting with storage buffer plus 10 mM reduced glutathione. The eluent
873 was dialyzed overnight against storage buffer, concentrated, snap-frozen, and stored in
874 aliquots at -80 °C.

875

876 ***PfFtsH1* enzymatic assays**

877 Rates of ATP hydrolysis by FtsH were measured using a coupled spectrophotometric
878 assay⁷² in PD buffer (25 mM HEPES, pH 7.5, 200 mM NaCl, 5 mM MgSO₄, 10 μM
879 ZnSO₄, 10% glycerol) with 3% dimethyl sulfoxide (DMSO) at 37 °C. Protein
880 degradation rates were measured by incubating FtsH (1 μM) with FITC-labeled casein (4
881 μM, Sigma, Type III) in PD buffer plus 3% DMSO. Reactions were started by adding

882 ATP (4 mM) with a regeneration system (16 mM creatine phosphate and 75 μ g/mL
883 creatine kinase), and degradation was followed by measuring the fluorescence intensity
884 (excitation 485 nm; emission 528 nm) at 37 °C. For activity-inhibition assays, reactions
885 were pre-incubated with inhibitor in DMSO for 10 min before adding ATP. Addition of
886 inhibitor provided the 3% DMSO found in the other assays. For determining specific
887 activities, the total concentration of casein was 10 μ M (2 μ M of FITC-labeled casein plus
888 8 μ M unlabeled casein).

889

890 **Statistical analysis**

891 When applicable, data was analyzed using Graph Pad Prism software and expressed as
892 mean values \pm standard error of the mean (SEM). Basic experiments were repeated at
893 least twice including both positive and negative controls. Biological replicates were
894 performed on different days or on independent cultures while technical replicates were
895 performed using cells from the same culture. Experiments were not blinded. All new
896 reagents were validated prior to use. All generated strains were checked for integration
897 using PCR, sequencing of the modified locus, western blot, and microscopy when
898 applicable. All qPCR primers were assessed for single amplicon.

899

900 **Data Availability**

901 Our research resources, including methods, cells, reagents and protocols, are available
902 upon request. Source data for the whole genome sequencing analysis is provided in
903 Extended Data Table 2.

904

- 905 63. Sidik, S. M. *et al.* A Genome-wide CRISPR Screen in *Toxoplasma* Identifies
906 Essential Apicomplexan Genes. *Cell* **166**, 1423–1435.e12 (2016).
907
- 908 64. Pfaffl, M. W. A new mathematical model for relative quantification in real-time RT-
909 PCR. *Nucleic Acids Res.* **29**, e45 (2001).
910
- 911 65. Shen, B., Brown, K. M., Lee, T. D. & Sibley, L. D. Efficient gene disruption in
912 diverse strains of *Toxoplasma gondii* using CRISPR/CAS9. *mBio* **5**, e01114-01114
913 (2014).
914
- 915 66. Camps, M. *et al.* A rRNA mutation identifies the apicoplast as the target for
916 clindamycin in *Toxoplasma gondii*. *Mol Microbiol.* **5**, 1309-18 (2002).
917
- 918 67. Dahl, E.L., Rosenthal, P.J. Multiple antibiotics exert delayed effects against the
919 *Plasmodium falciparum* apicoplast. *Antimicrob Agents Chemother.* **51**, 3485-90
920 (2007).
921
- 922 68. Striepen, B. *et al.* The plastid of *Toxoplasma gondii* is divided by association with
923 the centrosomes. *J Cell Biol.* **151**, 1423-1424 (2000).
924
- 925 69. Nkrumah L.J. *et al.* Efficient site-specific integration in *Plasmodium falciparum*
926 chromosomes mediated by mycobacteriophage Bxb1 integrase. *Nature Methods.*
927 **8**, 615-21 (2006).

928

929 70. Gubbels M.J. *et al.* High-throughput growth assay for *Toxoplasma gondii* using
930 yellow fluorescent protein. *Antimicrob Agents Chemother.* **47**, 309-16. (2003).

931

932

933 71. Gibson D.G. *et al.* Enzymatic assembly of DNA molecules up to several hundred
934 kilobases. *Nature Methods.* **6(5)**, 343-5. (2009).

935

936 72. Norby, J.G. Coupled assay of Na⁺, K⁺-ATPase activity. *Methods Enzymol.* **156**, 116-
937 9. (1988).

938

939 **Acknowledgements**

940 We thank Katrina Hong for assistance in drug assays, Dr. Boris Striepen for providing the
941 *T. gondii* FNR-RFP as well as tandem tomato strains, Drs. David Scheinberg and
942 Ouathek Ouerfelli for providing actinamide, and Dr. Saman Habib for providing *PfFtsH1*
943 antibody. This project has been funded with federal funds from the NIAID, NIGMS, and
944 Director's Fund, National Institutes of Health, Department of Health and Human Services
945 under Award Numbers 1K08AI097239 (EY), 1DP5OD012119 (EY), U19AI110819
946 (HAL), 1DP2OD007124 (JCN), P50 GM098792 (JCN), AI016892 (RTS),
947 F32GM116241 (SBH), and T32GM007276 (KAJ). Funding was also provided by the
948 Burroughs-Wellcome Fund (EY), Bill and Melinda Gates Foundation (OPP1069759;
949 JCN), and the Stanford Bio-X SIGF William and Lynda Steere Fellowship (KAJ).

950

951 **Author Information**

952 **Affiliations**

953 Department of Biochemistry, Stanford Medical School, Stanford, California 94305
954 Katherine Amberg-Johnson, Ellen Yeh

955

956 Department of Pathology, Stanford Medical School, Stanford, California 94305
957 Ellen Yeh

958

959 Department of Microbiology & Immunology, Stanford Medical School, Stanford,
960 California, 94305

961 Katherine Amberg-Johnson, Ellen Yeh

962

963 Department of Biology, Massachusetts Institute of Technology, Cambridge,
964 Massachusetts, 02139

965 Sanjay B. Hari, Robert T. Sauer

966

967 Department of Biological Engineering, Massachusetts Institute of Technology,
968 Cambridge, Massachusetts, 02139

969 Suresh M. Ganesan, Jacquin C. Niles

970

971 Department of Infectious Disease, The J. Craig Venter Institute, Rockville, Maryland,
972 20850

973 Hernan A. Lorenzi

974

975 **Contributions**

976 K.A-J. and E.Y. conceived and designed experiments. K.A-J. performed the majority of
977 the experiments. S.B.H. and R.T.S. conceived and designed the enzymatic experiments.
978 S.B.H purified PfFtsH1 and performed all the enzymatic assays. S.M.G. and J.C.N.
979 designed and generated the FtsH1 knockdown and PDF induction constructs. H.A.L.
980 performed the whole-genome sequencing and variant analysis. K.A-J. and E.Y. analyzed
981 the data and wrote the manuscript. All authors discussed and edited the manuscript.

982

983 **Competing financial interests**

984 The authors declare no competing financial interests.

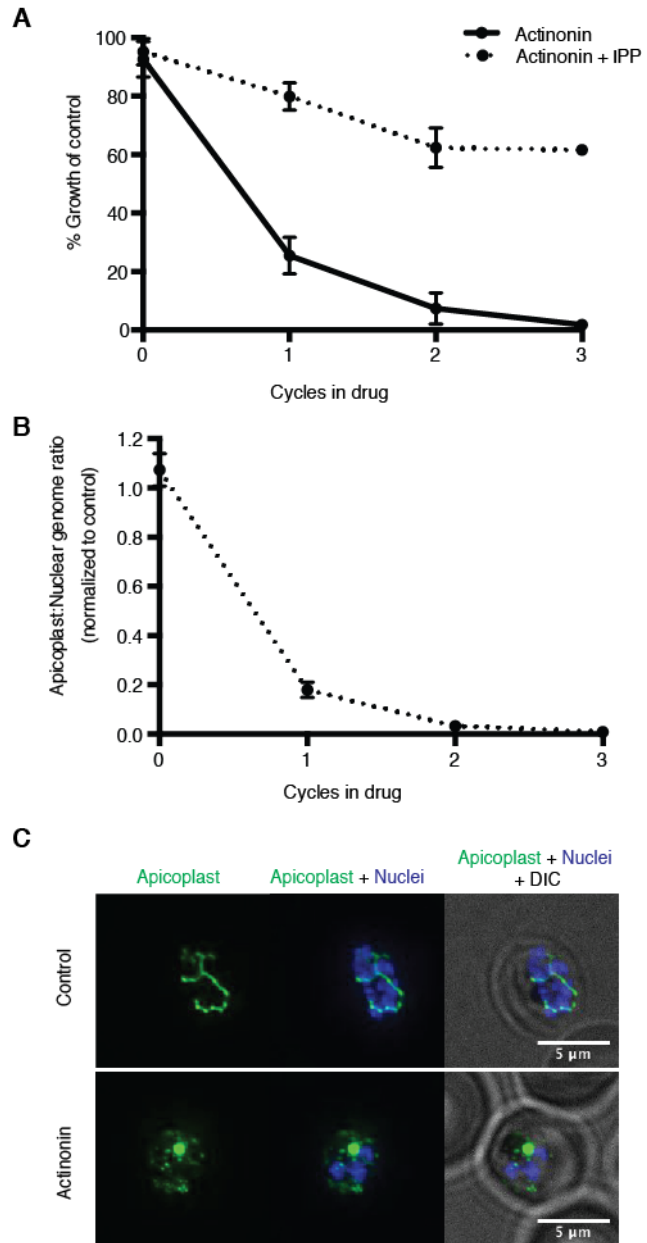
985

986 **Corresponding author**

987 Correspondence to: Ellen Yeh

988

989 **Fig 1: Actinonin inhibits apicoplast biogenesis in *P. falciparum***
990 **(a)** Time course of parasite growth during actinonin treatment with or without IPP, normalized to control cultures with or without IPP as appropriate. Error bars represent the SEM of two biological replicates.
991 **(b)** Time course of the apicoplast:nuclear genome ratio measured by quantitative PCR (qPCR) using primers for the apicoplast and nuclear genomes during treatment with actinonin and IPP. Genome ratios were normalized to control parasites grown with IPP only. Error bars as in **a**.
992 **(c)** Representative images of the apicoplast of IPP-rescued control and actinonin treated parasites 24 hours after treatment during the schizont stage. The apicoplast is visualized using the *P. falciparum* reporter strain D10 ACP-GFP in which GFP is targeted to the apicoplast and the nucleus is stained with Hoescht 33342. During *Plasmodium* replication, the apicoplast starts as a single small spherical organelle (ring stage) which branches and divides into multiple apicoplasts (schizont stage). A punctate apicoplast that does not branch indicates a defect in apicoplast biogenesis.
1000
1001
1002
1003
1004
1005
1006
1007
1008
1009
1010
1011
1012
1013
1014
1015
1016
1017
1018
1019
1020
1021
1022
1023
1024



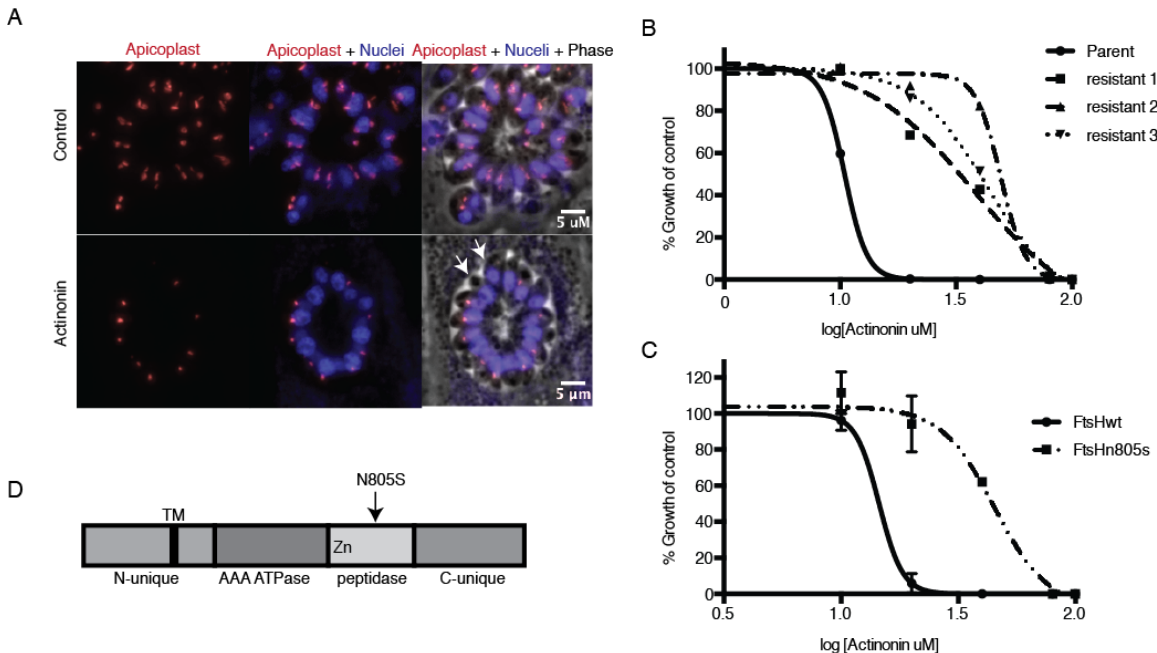
1025 **Fig 2: A mutation in the protease domain of *ftsH1* is sufficient to confer resistance to**
 1026 **actinonin in *T. gondii***

1027 (a) Representative images of the apicoplast of control and actinonin treated parasites 36
 1028 hours after infection. The apicoplast is visualized using the *T. gondii* reporter strain RH
 1029 FNR-RFP in which RFP is targeted to the apicoplast and the nucleus is stained with
 1030 Hoescht 33342. Each parasite contains one apicoplast, except during cell division when
 1031 there may be two. White arrows point at examples of *T. gondii* parasites missing an
 1032 apicoplast.

1033 (b) Dose-dependent parasite growth inhibition upon treatment with actinonin for the
 1034 actinonin-sensitive parent strain (RH) compared with 3 independent clones following
 1035 selection for actinonin resistance (resistant 1, resistant 2, resistant 3). These three
 1036 resistant clones are representative of the eight clones submitted for whole genome
 1037 sequencing. Growth was measured via summed areas of the plaques formed during
 1038 plaque assays and normalized to untreated controls. Error bars represent the SEM of two
 1039 biological replicates.

1040 (c) Dose-dependent parasite growth inhibition upon treatment with actinonin for *ftsH1*WT
 1041 compared with *ftsH1*(N805S) parasites in RH Δ ku80 strain. Data was measured and
 1042 analyzed as in 2b.

1043 (d) Schematic of TgFtsH1. This protein contains a N-unique region containing a putative
 1044 transmembrane domain, an AAA ATPase domain used for unfolding proteins, a
 1045 peptidase domain with a zinc co-factor in the catalytic site, and a C-unique region. The
 1046 resistance-conferring variant FtsH(N805S) is found in the peptidase domain near the
 1047 catalytic site.
 1048



1049

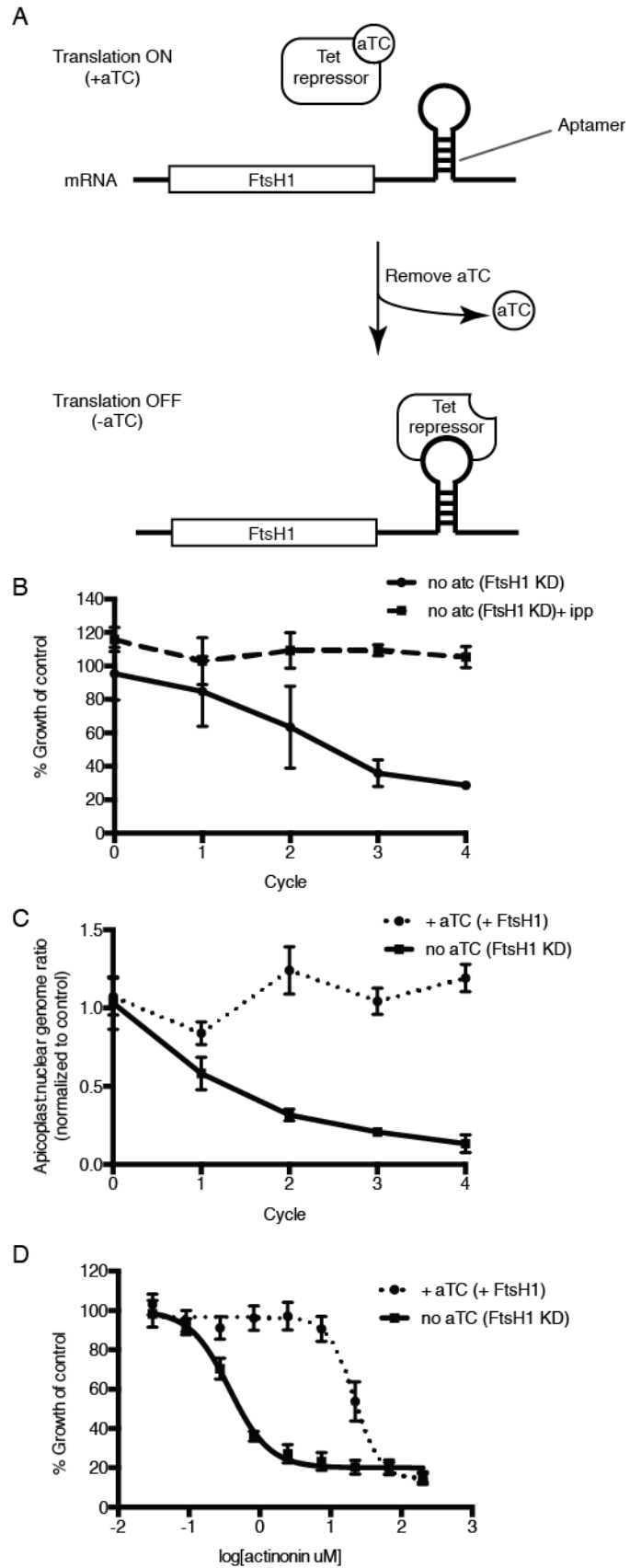
1050 **Fig 3: Knockdown of *ftsH1* in *P.***
 1051 ***falciparum* leads to apicoplast**
 1052 **loss and hypersensitivity to**
 1053 **actinonin**

1054 (a) Schematic of the endogenous
 1055 knockdown strategy. When aTC is
 1056 present in the media, the tet-
 1057 repressor binds aTC and does not
 1058 bind the 10x-aptamer sequence,
 1059 which relieves translational
 1060 repression, allowing PfFtsH1 to be
 1061 expressed. When aTC is washed
 1062 out of the media, the tet-repressor
 1063 binds the 10x-aptamer and
 1064 prevents expression of PfFtsH1.

1065 (b) Time course of parasite growth
 1066 without aTC and in the presence or
 1067 absence of IPP in the media,
 1068 normalized to the untreated or IPP-
 1069 rescued parental strain as
 1070 appropriate. Error bars represent
 1071 the SEM of two biological
 1072 replicates.

1073 (c) Time course of the
 1074 apicoplast:nuclear genome ratio
 1075 measured by quantitative PCR
 1076 (qPCR) using primers for the
 1077 apicoplast and nuclear genomes
 1078 during treatment with or without
 1079 aTC. All samples contained IPP to
 1080 rescue parasite growth. Genome
 1081 ratios were normalized to
 1082 respective parental cultures also
 1083 grown with IPP. Error bars as in c.

1084 (d) Dose-dependent parasite
 1085 growth inhibition by actinonin in
 1086 the absence or presence of aTC.
 1087 Error bars as in c.



1093 **Figure 4: Actinonin inhibits *PfFtsH1* in vitro.**

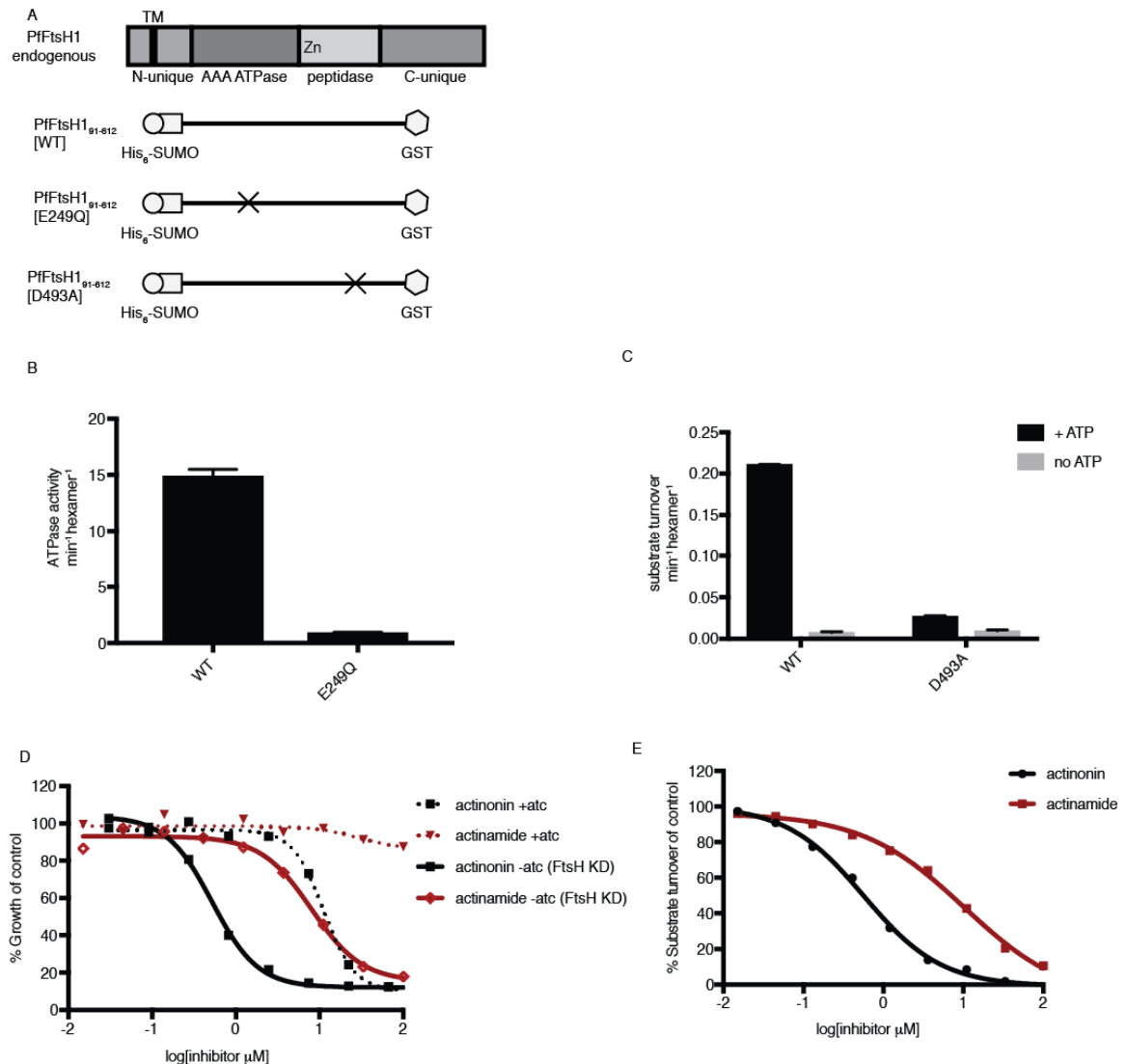
1094 (a) Schematic of *PfFtsH1* constructs used for biochemical assays. Amino acids 91-612 of
1095 the endogenous protein (*PfFtsH1* endogenous), which include the AAA+ ATPase and
1096 peptidase domains, were placed between His₆-SUMO and GST domains to aid in
1097 purification and solubility. WT is the parent construct, E249Q is an inactivating mutation
1098 in the AAA+ ATPase domain, and D493A is an inactivating mutation in the peptidase
1099 domain.

1100 (b) ATP hydrolysis by *PfFtsH1* WT and E249Q measured using a coupled
1101 spectrophotometric assay⁷².

1102 (c) ATP-dependent proteolysis of FITC-labeled casein by *PfFtsH1* WT and D493A.

1103 (d) Dose-dependent parasite growth inhibition by actinonin (black) or actinamide (red)
1104 with and without knockdown of *PfFtsH1*. Error bars represent the SEM of two biological
1105 replicates.

1106 (e) Dose-dependent proteolytic inhibition of FITC-labeled casein by *PfFtsH1* WT. Error
1107 bars represent the SEM of 3 replicates.
1108



1109

1110 **Extended Data 1: Actinonin**
1111 **specifically inhibits the apicoplast of**
1112 ***P. falciparum* leading to parasite**
1113 **death after a single replication cycle**
1114 (a) Dose-dependent parasite growth
1115 inhibition by actinonin in the absence
1116 or presence of IPP. Error bars
1117 represent the standard error of the
1118 mean (SEM) of two biological
1119 replicates.

1120 (b) Time course of parasite growth
1121 during treatment with actinonin,
1122 chloramphenicol, or fosmidomycin in
1123 the absence or presence of IPP.
1124 Growth is normalized to untreated or
1125 IPP-rescued controls as appropriate.
1126 Error bars as in a. In contrast to other
1127 antimalarials, which cause growth
1128 inhibition in a single replication cycle,
1129 “delayed death” in *P. falciparum* is
1130 associated with inhibitors of apicoplast
1131 gene expression and has previously been described in detail⁶⁷. It is characterized by a
1132 normal apicoplast and cell division during drug treatment for one replication cycle,
1133 followed by halted apicoplast and cell division in daughter parasites of drug-treated
1134 parasites.

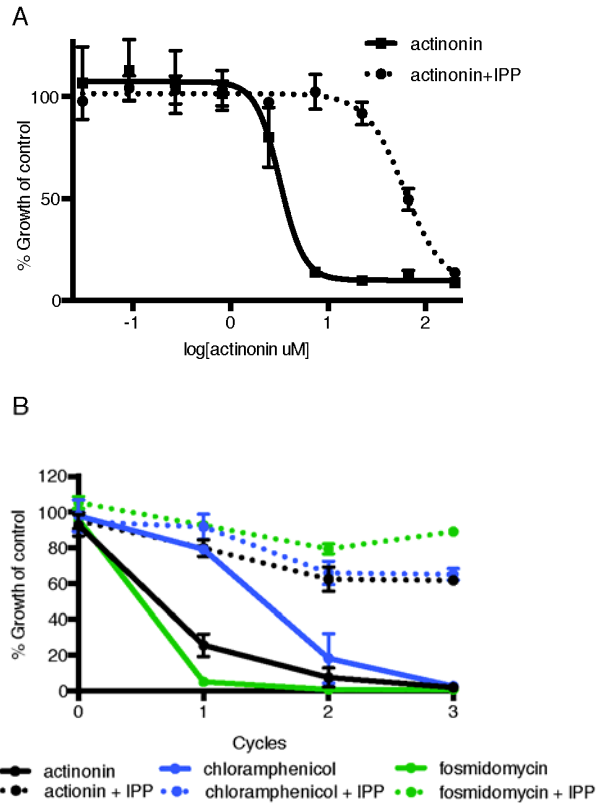
1135

1136

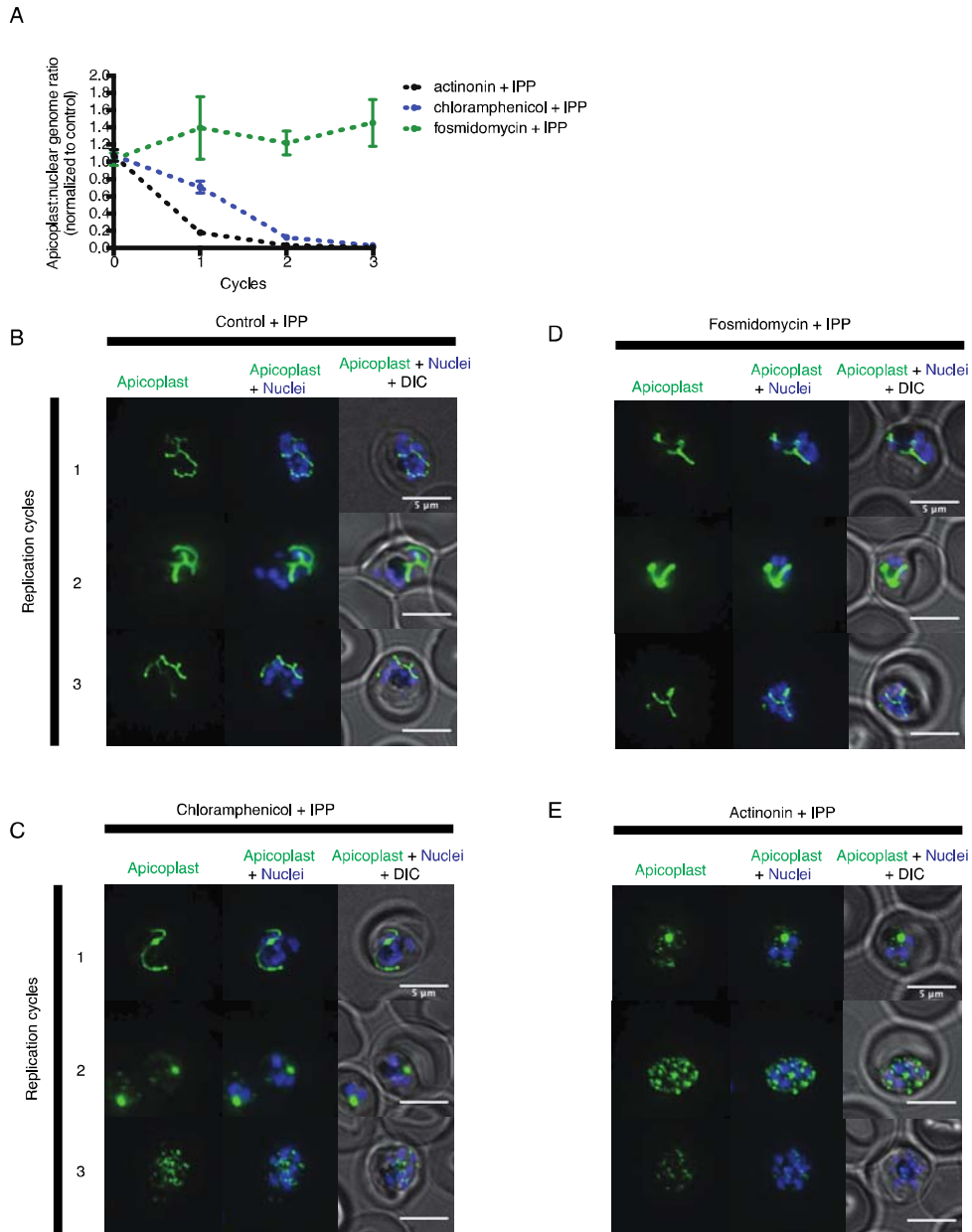
1137 **Extended Data Fig 2: Actinonin has a distinct inhibition phenotype compared to**
1138 **inhibitors of apicoplast metabolism and translation**

1139 (a) Time course of the apicoplast:nuclear genome ratio measured by quantitative PCR
1140 (qPCR) for targets in the apicoplast and nuclear genome during treatment with actinonin
1141 (black), chloramphenicol (blue), or fosmidomycin (green). While actinonin treatment
1142 blocks apicoplast genome replication in a single replication cycle, this effect is not
1143 observed until the second replication cycle of chloramphenicol treatment and not at all
1144 during fosmidomycin treatment. This is consistent with actinonin blocking apicoplast
1145 biogenesis, chloramphenicol blocking apicoplast translation leading to a delayed
1146 apicoplast biogenesis defect, and fosmidomycin blocking apicoplast metabolic function
1147 but not biogenesis. All samples were grown in IPP and genome ratios were normalized to
1148 the untreated control cultures also containing IPP. Error bars represent the SEM of at
1149 least 2 biological replicates.

1150 (b-e) Representative images of the apicoplast during schizont stage of three successive
1151 replication cycles in untreated (b), chloramphenicol (c), fosmidomycin (d) and actinonin
1152 (e) treated cultures all grown with IPP. The apicoplast is visualized using the *P.*
1153 *falciparum* reporter strain D10 ACP-GFP in which GFP is targeted to the apicoplast and
1154 the nucleus is stained with Hoescht 33342. In this case, a branched apicoplast indicates



1155 successful apicoplast development while punctate apicoplasts (observed in replication
1156 cycle 1 for actinonin treatment (e) and replication cycle 2 for chloramphenicol treatment
1157 (c)) represents an apicoplast that has failed to develop. The apicoplast is no longer
1158 present after replication cycle 2 of actinonin treatment and upon replication cycle 3 of
1159 chloramphenicol treatment, which leads to complete mislocalization of the GFP.
1160



1161

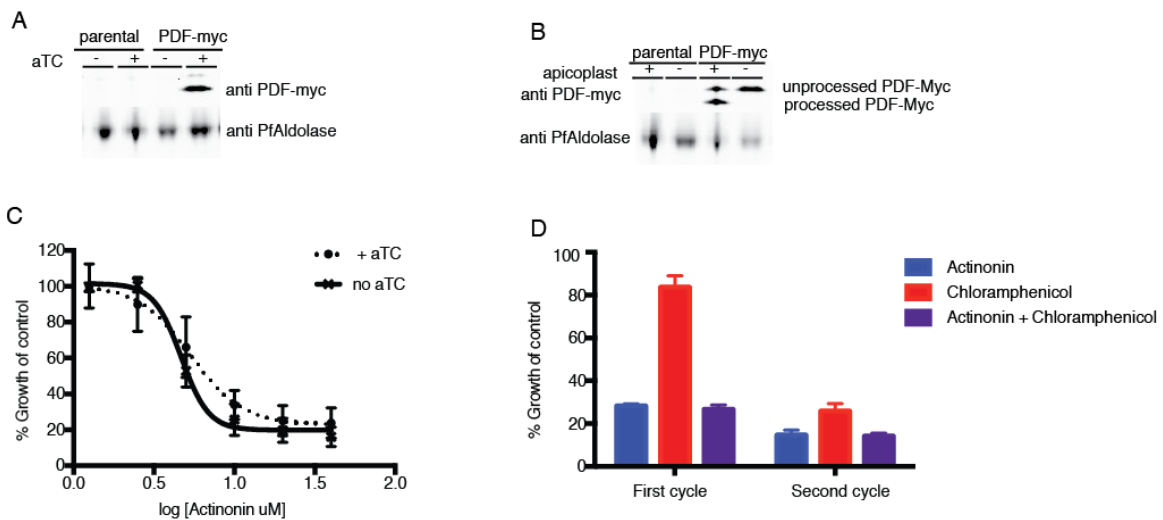
1162 **Extended Data Fig 3: Actinonin is unlikely to inhibit the peptide deformylase of *P.***
 1163 ***falciparum***

1164 (A) Western blot of the parental line (NF54attB-pCRISPR) and the PDF-myc parasites
 1165 grown with or without aTC for 24 hours. Induction of the second copy of PfPDF (PDF-
 1166 myc) with 4uM aTC results in two bands, the top lighter band representing unprocessed
 1167 PDF-myc, and the bottom darker band representing processed PDF-myc. PfAldolase is
 1168 used as a loading control. Induction with 0.125-4uM aTC results in similar amount of
 1169 PDF-myc induction (data not shown).

1170 (B) Western blot for PDF-myc of parasites with or without their apicoplast. An
 1171 accumulation of unprocessed PDF-myc is observed when the apicoplast is missing, due
 1172 to loss of the transit peptide cleavage that usually occurs upon import to the apicoplast.
 1173 This has been shown previously for apicoplast-resident proteins and is consistent
 1174 apicoplast localization⁸.

1175 (C) Dose dependent parasites growth inhibition by actinonin in the presence of 4uM aTC
 1176 does not change the actinonin EC₅₀. This experiment was also performed under IPP
 1177 rescue conditions, to confirm apicoplast specificity of actinonin and with a range of aTC
 1178 concentrations (0.125-4uM) to insure max expression of PDF-myc (data not shown).
 1179 Error bars represent the SEM of 3 biological replicates.

1180 (D) Parasite growth after one or two replication cycles after treatment with actinonin,
 1181 chloramphenicol, or both actinonin and chloramphenicol normalized to growth of an
 1182 untreated control. Treatment with actinonin alone inhibited growth after the first
 1183 replication cycle, whereas treatment with chloramphenicol alone inhibited growth after
 1184 the second replication cycle. Co-treatment with chloramphenicol, which targets
 1185 apicoplast translation, did not suppress effects of actinonin treatment, which was
 1186 inconsistent with actinonin targeting the peptide deformylase (PDF) of the apicoplast.
 1187 This experiment was tried using a range of concentrations of actinonin and
 1188 chloramphenicol to insure the data was not the result of partial inhibition. All
 1189 concentrations that lead to apicoplast-specific death gave this phenotype (data not
 1190 shown).
 1191

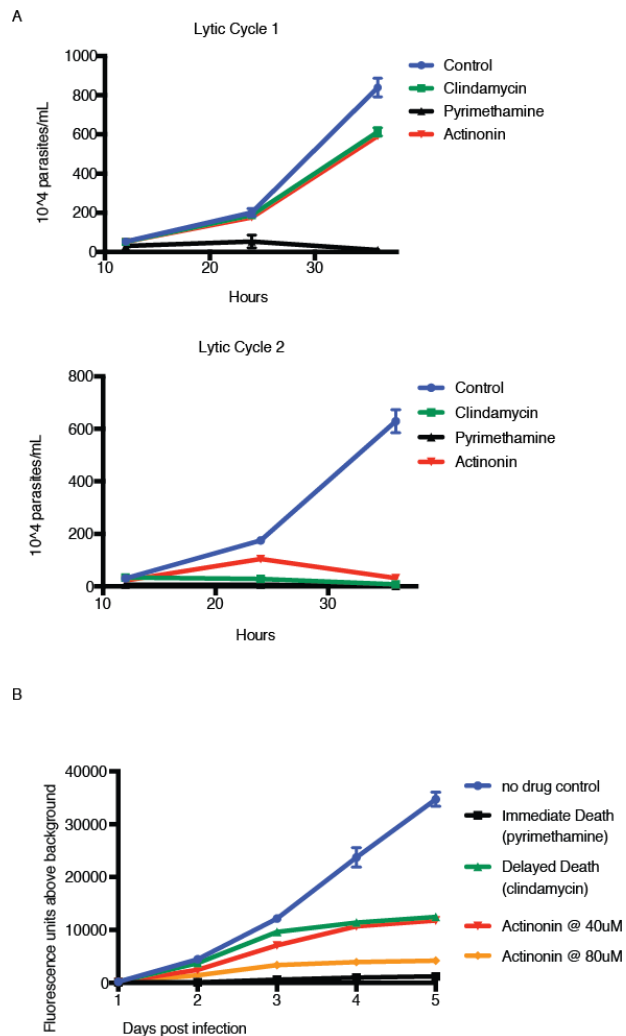


1192
 1193

1194

1195 **Extended Data Fig 4: Actinonin**
1196 **treatment causes “delayed death” in**
1197 ***T. gondii* associated with apicoplast**
1198 **loss**

1199 (A) Time course of parasite growth of
1200 untreated (blue), clindamycin (green),
1201 pyrimethamine (black), or actinonin
1202 (red) treated parasites over the course
1203 of two lytic cycles. Unlike *P.*
1204 *falciparum*, *T. gondii* undergoes
1205 multiple replication cycles in the host
1206 cell before lysis, thus each *T. gondii*
1207 lytic cycle represents multiple parasite
1208 replication cycles. Pyrimethamine
1209 inhibits parasite dihydrofolate
1210 reductase and was used as a control for
1211 a non-apicoplast targeting drug that
1212 inhibits growth in a single lytic cycle.
1213 As previously reported⁶⁶, clindamycin,
1214 an apicoplast translation inhibitor,
1215 gave a “delayed death” phenotype in *T.*
1216 *gondii* characterized by completed cell
1217 divisions and host re-invasion during
1218 drug treatment in the first lytic cycle,
1219 followed by halted cell division in the
1220 second lytic cycle. Actinonin also led
1221 to growth inhibition in the second lytic
1222 cycle, suggesting that it also targets the
1223 apicoplast. Error bars represent the
1224 SEM of two biological replicates. It is important to distinguish between apicoplast-
1225 associated “delayed death” in *P. falciparum* and that in *T. gondii*. In *T. gondii*, apicoplast
1226 loss occurs in the first lytic cycle and is temporally separate from defects in parasite cell
1227 division and growth inhibition observed in the second lytic cycle; whereas in *P.*
1228 *falciparum* defects in apicoplast biogenesis, parasite cell division, and growth inhibition
1229 all occur in the second replication cycle. “Delayed death” in *T. gondii* therefore appears
1230 more broadly associated with disruption of apicoplast biogenesis, where “delayed
1231 death” in *P. falciparum* appears more specific to disruption of apicoplast gene expression
1232 that leads to delayed biogenesis defects.
1233 (B) To determine dose-dependent drug target specificity, we used a previously described
1234 fluorescent growth assay to quantify the kinetics of death in *T. gondii*⁷⁰. Briefly, *T. gondii*
1235 expressing tandem-tomato are treated with drug and fluorescence is quantified daily as a
1236 proxy of parasite replication. While 40uM actinonin leads to delayed-death kinetics
1237 similar to clindamycin, 80uM actinonin results in immediate death kinetics similar to
1238 pyrimethamine, indicating that at this concentration, actinonin hits a second, non-
1239 apicoplast target.



1240

1241 **Extended Data Fig 5: C-terminal**
1242 **cleavage of PfFtsH1 is dependent**
1243 **on the presence of the apicoplast**
1244 **and efficiency of PfFtsH1 knock-**
1245 **down can be assessed in parasites**
1246 **missing their apicoplast.**

1247 (A) Western blot of *PfFtsH*-FLAG
1248 levels in parasites with and without
1249 an apicoplast and with and without
1250 aTC induction. Consistent with the
1251 previous report of *PfFtsH1* C-
1252 terminal processing, we were unable
1253 to detect full-length *PfFtsH1*-FLAG
1254 using anti-FLAG in parasites with
1255 intact apicoplasts (lane 1)^{37,40}.

1256 However, in parasites missing apicoplasts, full-length *PfFtsH1*-FLAG was detectable,
1257 suggesting that *PfFtsH1* processing requires the apicoplast (lanes 2). *PfFtsH1*-FLAG is
1258 not observed in parasites with or without apicoplasts if there is no aTC induction,
1259 indicating that the band representing FtsH-FLAG is specific and not an artifact of missing
1260 apicoplasts (lanes 3-4 respectively). All samples contain IPP to rescue growth and Cas9-
1261 FLAG is used as a loading control. Each sample was taken at the trophozoite stage.

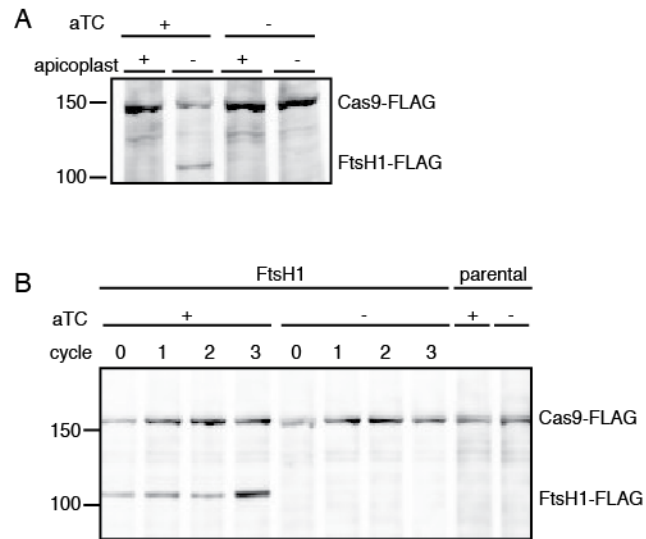
1262 (B) To assess the knockdown efficiency of *PfFtsH1*, we used a western blot comparing
1263 *PfFtsH1*-FLAG levels in the presence (lanes 1-4) or absence of aTC (lanes 5-8) in IPP-
1264 rescued parasites missing their apicoplast. Each sample was taken at the trophozoite stage
1265 and cycle 0 indicates 24 hours after the removal of aTC. Lanes 9 and 10 are samples from
1266 the parental strain that do not contain the FLAG-tag or the aptamer sequence in the 3'
1267 UTR of *PfFtsH1*. In each case, Cas9-FLAG was used as a loading control. *PfFtsH1*-
1268 FLAG levels were reduced to undetectable levels at 24 hours after aTC removal,
1269 validating our knockdown strategy.

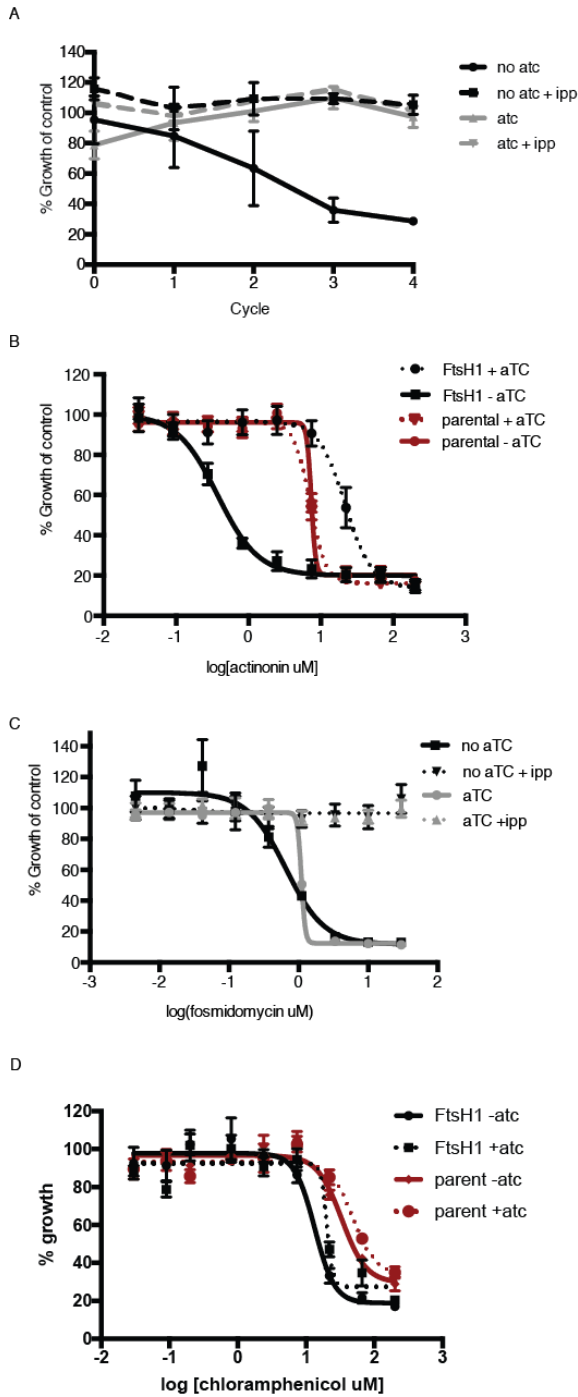
1270

1271

1272

1273





Extended Data Fig 6: Knockdown of *PfFtsH1* specifically disrupts the apicoplast and leads to specific hypersensitivity to actinonin

(a) Time course of parasite growth with or without aTC and with or without IPP in the media. IPP rescues the growth defect observed in upon *PfFtsH1*

downregulation, indicating that *PfFtsH1* is essential for an apicoplast-specific function. Growth is shown normalized to the untreated or IPP-rescued parental strain as appropriate. Error bars represent the SEM of two biological replicates.

(b) Dose-dependent parasite growth inhibition by actinonin with or without aTC for the parental (red) and *PfFtsH1* (black) strain. The EC_{50} of the parental strain is unchanged by the removal of aTC. Error bars as in **a**.

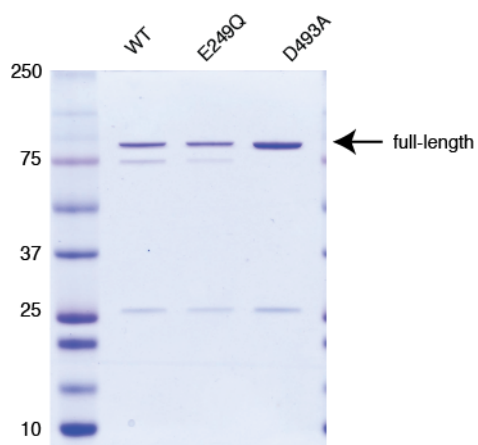
(c) Dose-dependent parasite growth inhibition by fosmidomycin with or without aTC and with or without IPP. The fosmidomycin EC_{50} is unchanged by regulating levels of *PfFtsH1*, indicating that the observed hypersensitivity to actinonin upon knockdown of *PfFtsH1* is specific to actinonin and does not occur for all apicoplast drug. Error bars represent the SEM of three technical replicates.

(d) Dose-dependent parasites growth inhibition by chloramphenicol during the second lytic cycle (120 h) with or without aTC. Error bars represent the SEM of three technical replicates. The chloramphenicol EC_{50} is unchanged by regulating levels of *PfFtsH1*, indicating

1312 that the observed hypersensitivity to actinonin upon knockdown of *PfFtsH1* is specific to
 1313 actinonin and does not occur for all apicoplast drugs.

1314
 1315

1316 **Extended Data Fig 7: Purification of *Pf*FtsH1.** Purified samples were separated by
1317 SDS-PAGE and stained with Coomassie. Full-length product is 97 kDa.
1318



1319